ELECTRONIC SUPPLEMENTARY INFORMATION

Boosting axiality in stable high-coordinate Dy(III) single-molecule magnets

Angelos B. Canaj,[a] Mukesh Kumar Singh,[b] Emma Regincós Marti,[a] Marko Damjanović,[c] Claire Wilson,[a] Oscar Céspedes,[d] Wernsdorfer Wolfgang,[c] Gopalan Rajaraman*[b] and Mark Murrie*[a]

[a] WestCHEM, School of Chemistry, University of Glasgow, University Avenue, Glasgow, G12 8QQ, UK.E-mail: Mark.Murrie@glasgow.ac.uk

[b] Department of Chemistry, Indian Institute of Technology Bombay, Powai, Mumbai, Maharashtra, 400076, India. E-mail: rajaraman@chem.iitb.ac.in.

[c] Physikalisches Institut (PHI), Karlsruhe Institute of Technology, Wolfgang-Gaede-Strasse 1, 76131 Karlsruhe, Germany. Institute of Nanotechnology (INT), Karlsruhe Institute of Technology, Hermann-von-Helmholz-Platz 1, 76344 Eggenstein-Leopoldshafen, Germany.

[d] School of Physics and Astronomy, University of Leeds, Leeds LS2 9JT, UK.

Materials and physical measurements

All manipulations were performed under aerobic conditions, using materials as received. Elemental analyses (C, H, N) were performed by the University of Glasgow microanalysis service. The preparation of 1,4,7,10-tetrakis(2-pyridylmethyl)-1,4,7,10-tetraaza-cyclododecane (L) was performed following a similar synthesis used in the literature.[1] The synthesis of the ligands were conducted under an argon atmosphere with rigorous exclusion of oxygen and water using Schlenk line and glove box techniques. Variable-temperature, solid-state direct current (dc) magnetic susceptibility data down to 2.0 K were collected on a Quantum Design SQUID-VSM magnetometer at the University of Leeds. Polycrystalline samples were embedded in eicosane and diamagnetic corrections were applied to the observed paramagnetic susceptibilities using Pascal's constants. Powder XRD measurements were collected on freshly prepared samples of **1** and **3** on a PANalytical X'Pert Pro MPD diffractometer (λ (CuKα_1) = 1.5405 Å) on a mounted bracket sample stage, at the University of Glasgow. Single Crystal X-Ray diffraction data were collected using a Bruker D8 VENTURE diffractometer equipped with a Photon II CPAD detector, with an Oxford Cryosystems N-Helix device mounted on an IμS 3.0 (dual Cu and Mo) microfocus sealed tube generator at the University of Glasgow. Ultra-low temperature (<1.8 K) hysteresis studies were performed on a single crystal sample of **1** using an array of micro-SQUIDS (the field is oriented along the easy axis, which is found *in situ* by changing the field orientation with three coils).[2] Thermogravimetric analysis was performed on a SDT Q600 with an argon atmosphere (100 ml min^{-1}) in the 20 - 800 K temperature range (10 K min^{-1}), at the University of Glasgow. ^{1}H NMR spectra were recorded at 298.2 K on a Bruker AVIII 500 MHz spectrometer at the the University of Glasgow.

Synthesis

Synthetic strategy applicable to **1-3***:*

1,4,7,10-tetrakis(2-pyridylmethyl)-1,4,7,10-tetraaza-cyclododecane (43 mg, 0.08 mmol) was dissolved in 10 ml of methanol and was refluxed for 24 hours in the presence of $Dy(CF_3SO_3)_3$ (50 mg, 0.08 mmol). The reaction mixture was dried under vacuum and then dissolved in 10 ml of acetonitrile. The acetonitrile solution was refluxed for 3 hours and then dried under vacuum. The oily product was dissolved in hot dichloromethane (10 ml). The reaction mixture in dichloromethane was dried under vacuum giving a crude solid. Reaction of the solid with NH_4F in 5 ml of deionized H_2O and heating at 100 ^oC gives a clear solution. Colourless single

crystals of $[Dy^{III}LF](CF_3SO_3)_2 \cdot H_2O$ (**1**) (L= 1,4,7,10-tetrakis(2-pyridylmethyl)-1,4,7,10-tetraaza-cyclododecane) were isolated in ~ 10-15 % yield from the slow evaporation of the H_2O solution. The same procedure was followed for the isolation of $[La^{III}LF](CF_3SO_3)_2 \cdot H_2O$ (**2**) using $La(CF_3SO_3)_3$ (50 mg, 0.08 mmol) and **3** using $La(CF_3SO_3)_3$ (45 mg, 0.076 mmol) and $Dy(CF_3SO_3)_3$ (2.4 mg, 0.004 mmol).

Elemental Anal. calcd (found) for **1**: C 39.48 (39.39), H 4.09 (4.08), N 10.83 (10.78) %. **2**: C 40.47 (40.52), H 4.18 (4.13), N 11.03 (11.1) % **3**: C 40.4 (40.44), H 4.19 (4.10), N 11.09 (11.01) %.

*Synthetic strategy for **4**:*

6,6',6'',6'''-((1,4,7,10-tetraazacyclododecane-1,4,7,10-tetrayl)tetrakis(methylene))-tetrapicolinonitrile (**4**) : In a Schleck line and under argon atmosphere, cyclen (650 mg, 3.80 mmol) and Cs_2CO_3 (25 g mg 76.5 mmol) were mixed in 30 ml of anhydrous MeCN. Then, 6-(chloromethyl)picolinonitrile (2.3 g, 15.3 mmol) was dissolved in 30 ml of anhydrous MeCN and the yellow solution was transferred using a syringe into the mixture of cyclen and Cs_2CO_3. The obtained reaction mixture was refluxed under an argon atmosphere for 24 hours giving a brown solution with precipitate. The mixture was filtered and washed with hot DCM and MeCN. The combined filtered DCM and MeCN solution was dried under reduced pressure. The crystalline powder was recrystallized from MeCN giving crystals of **4** in good yields.

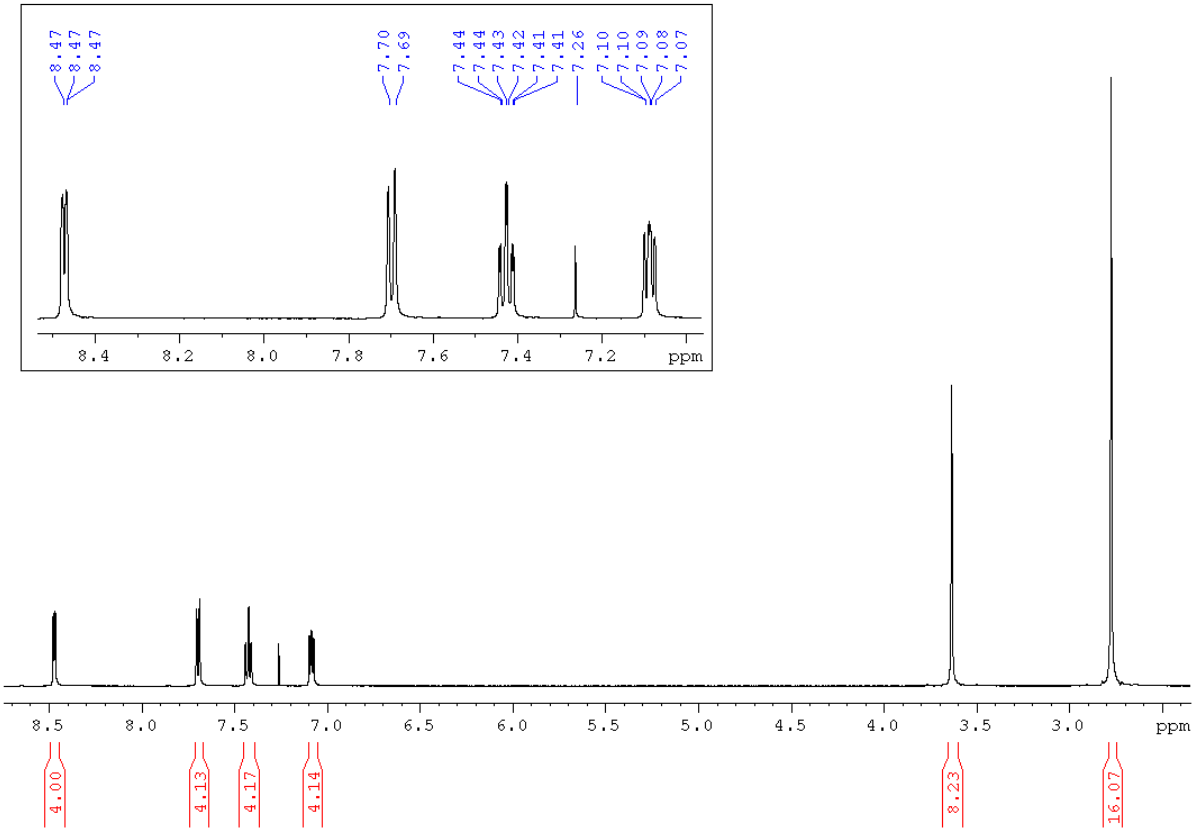

Fig. S1 ^{1}H NMR of the ligand, L, in $CDCl_3$: δ 2.77 (16 H, s, NC$\underline{H}_2$C$\underline{H}_2$N), 3.63 (8 H, s, NC$\underline{H}_2$(C_5H_4N)), 7.08 (4 H, ddd, J = 12.30 Hz, J = 7.8 Hz, J = 1.2 Hz, $C_5\underline{H}_4N$), 7.42 (4 H, td, J = 7.8 Hz, J = 1.2 Hz, $C_5\underline{H}_4N$)), 7.69 (4 H, d, J = 7.8 Hz, $C_5\underline{H}_4N$)), 8.47 (4 H, dd, J = 4.9 Hz, J = 1.2 Hz, $C_5\underline{H}_4N$), 7.26 ($CHCl_3$, s, solvent).

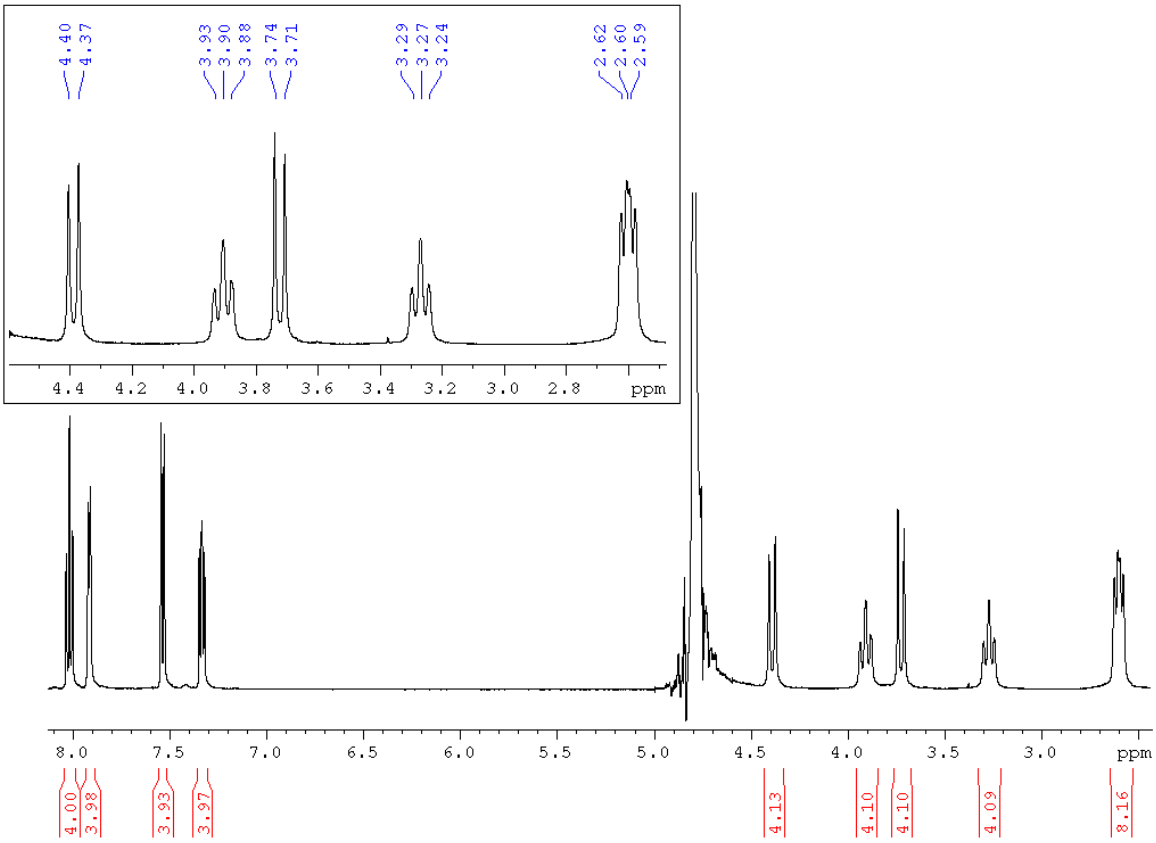

Fig. S2 ^{1}H NMR of **2** in D_2O: δ 2.60 (8 H, dd, J = 13.1 Hz, J = 9.2 Hz, NC$\underline{H}_2$(C_5H_4N)), 3.27 (ppm, 4 H, t, J = 13.1 Hz, NC$\underline{H}_2$C$\underline{H}_2$N), 3.72 (4 H, d, J = 16.2 Hz, NC$\underline{H}_2$C$\underline{H}_2$N), 3.90 (4 H, t, J = 13.1 Hz, NC$\underline{H}_2$C$\underline{H}_2$N), 4.38 (4 H, d, J = 16.2 Hz, NC$\underline{H}_2$C$\underline{H}_2$N), 7.33 (4 H, dd, J = 7.8 Hz, J = 5.7 Hz, $C_5\underline{H}_4$N), 7.53 (4 H, d, J = 7.8 Hz, $C_5\underline{H}_4$N)), 7.91 (4 H, d, J = 5.7 Hz, $C_5\underline{H}_4$N)), 8.02 (4 H, td, J = 7.8 Hz, J = 1.7 Hz, $C_5\underline{H}_4$N)), 4.79 (H_2O, s, solvent).

Table S1. Crystallographic data for complexes **1** and **2**. Note that **1** and **2** are isostructural but have different crystal cell parameters and crystallise in different space groups.[3]

	1	**2**
Formula	$C_{32}H_{40}DyFN_8{\cdot}2(CF_3O_3S){\cdot}H_2O$	$C_{32}H_{40}FLaN_8{\cdot}2(CF_3O_3S){\cdot}H_2O$
M_W	1034.37	1010.78
Crystal System	Orthorhombic	Orthorhombic
Space group	$P2_12_12$	*Pccn*
a/Å	11.3416 (5)	21.592 (3)
b/Å	21.5398 (8)	11.4165 (10)
c/Å	7.7573 (3)	15.9216 (16)
$\alpha/^o$	90	90
$\beta/^o$	90	90
$\gamma/^o$	90	90
V/Å^3	1895.08 (13)	3924.8 (7)
Z	2	4
T/K	150	150
λ/Å	0.71073	0.71073
D_c/g cm^{-3}	1.813	1.711
μ(Mo-K$_\alpha$)/ mm^{-1}	2.18	1.29
Meas./indep.(R_{int}) refl.	14716/4322 (0.034)	19906/4886(0.036)
Obs. refl. [$I>2\sigma(I)$]	4160	3940
$wR(F^2)$	0.049	0.087
$R[F^2 > 2s(F^2)]$	0.021	0.031
S	1.01	1.03
$\Delta\rho_{max,min}$/ eÅ^{-3}	0.76, -0.60	0.95, -1.23

Table S2. Crystallographic data for ligand **4**.[3]

	4
Formula	$C_{36}H_{36}N_{12}$
M_W	636.77
Crystal System	Monoclinic
Space group	$P2_1/c$
a/Å	11.7725 (7)
b/Å	6.3142 (3)
c/Å	21.5298 (13)
α/°	90
β/°	94.186 (2)
γ/°	90
V/Å^3	1596.12 (16)
Z	2
T/K	150
λ/Å	0.71073
D_c/g cm^{-3}	1.325
μ(Mo-K$_\alpha$)/ mm^{-1}	0.08
Meas./indep.(R_{int}) refl.	17399/3946
Obs. refl. [$I>2\sigma(I)$]	2711
$wR(F^2)$	0.126
$R[F^2 > 2s(F^2)]$	0.050
S	1.03
$\Delta\rho_{max,min}$/ eÅ^{-3}	0.22, -0.26

Table S3. Selected bond distances and angles for complex **1** (Å, º).[3]

Dy1—N2^{i}	2.689 (3)	Dy1—N4^{i}	2.531 (3)
Dy1—N2	2.689 (3)	Dy1—N3	2.541 (3)
Dy1—N1^{i}	2.669 (3)	Dy1—N3^{i}	2.541 (3)
Dy1—N1	2.669 (3)	Dy1—F1	2.123 (2)
Dy1—N4	2.531 (3)		
N2^{i}—Dy1—N2	103.02 (13)	N4—Dy1—N2	73.69 (10)
N1—Dy1—N2	67.31 (9)	N4^{i}—Dy1—N2	129.64 (10)
N1—Dy1—N2^{i}	67.52 (9)	N4^{i}—Dy1—N1^{i}	65.16 (10)
N1^{i}—Dy1—N2	67.52 (9)	N4—Dy1—N1^{i}	140.72 (10)
N1^{i}—Dy1—N2^{i}	67.31 (9)	N4^{i}—Dy1—N1	140.72 (10)
N1—Dy1—N1^{i}	103.81 (13)	N4—Dy1—N1	65.16 (10)
N4^{i}—Dy1—N2^{i}	73.69 (10)	N4—Dy1—N4^{i}	146.66 (15)
N4—Dy1—N2^{i}	129.64 (10)	N4—Dy1—N3^{i}	86.36 (11)
N4—Dy1—N3	84.34 (11)	F1—Dy1—N2	128.49 (7)
N4^{i}—Dy1—N3^{i}	84.34 (11)	F1—Dy1—N2^{i}	128.49 (7)
N3^{i}—Dy1—N2^{i}	64.77 (10)	F1—Dy1—N1	128.10 (7)
N3—Dy1—N2^{i}	141.07 (9)	F1—Dy1—N1^{i}	128.10 (7)
N3^{i}—Dy1—N2	141.07 (9)	F1—Dy1—N4^{i}	73.33 (8)
N3—Dy1—N2	64.77 (10)	F1—Dy1—N4	73.33 (8)
N3^{i}—Dy1—N1	74.04 (10)	F1—Dy1—N3^{i}	73.59 (7)
N3^{i}—Dy1—N1^{i}	128.58 (10)	F1—Dy1—N3	73.59 (7)
N3—Dy1—N1^{i}	74.04 (10)	N3—Dy1—N1	128.58 (10)
N3^{i}—Dy1—N3	147.18 (15)		

Symmetry code: i) -*x*+1, -*y*+1, *z*; (ii) -*x*, -*y*+1, *z*.

Table S4. Shape measures of complex **1**. The lowest CShMs value, is highlighted.[4]

	Dy	**Symmetry**	**Ideal polyhedron**
EP-9	37.272	D9h	Enneagon
OPY-9	20.481	C8v	Octagonal pyramid
HBPY-9	19.176	D7h	Heptagonal bipyramid
JTC-9	17.679	C3v	Johnson triangular cupola J3
JCCU-9	9.704	C4v	Capped cube J8
CCU-9	7.412	C4v	Spherical-relaxed capped cube
JCSAPR-9	2.435	C4v	Capped square antiprism J10
JTCTPR-9	4.037	D3h	Tricapped trigonal prism J51
TCTPR-9	1.485	D3h	Spherical tricapped trigonal prism
JTDIC-9	12.672	C3v	Tridiminished icosahedron J63
HH-9	12.513	C2v	Hula-hoop
MFF-9	**1.429**	**Cs**	**Muffin**

Table S5. Shape measures of the {DyN_8} core found in **1**. The lowest CShMs value, is highlighted.[4]

	Dy	**Symmetry**	**Ideal polyhedron**
OP-8	22.611	D8h	Octagon
HPY-8	26.199	C7v	Heptagonal pyramid
HBPY-8	17.277	D6h	Hexagonal bipyramid
CU-8	9.724	Oh	Cube
SAPR-8	**1.411**	**D4d**	**Square antiprism**
TDD-8	3.663	D2d	Triangular dodecahedron
JGBF-8	16.756	D2d	Johnson gyrobifastigium J26
JBTPR-8	3.408	C2v	Biaugmented trigonal prism J50
BTPR-8	2.045	C2v	Biaugmented trigonal prism
JSD-8	6.330	D2d	Snub diphenoid J84
TT-8	10.585	Td	Triakis tetrahedron
ETBPY-8	22.875	D3h	Elongated trigonal bipyramid

Table S6. High coordinate Dy(III) Single Ion Magnets.

Complex	U_{eff} (K)	τ_o (s)	Coord. Number	Dc applied field (Oe)	Ref.
$[(L^1)Dy(NO_3)_2(H_2O)_2]C_2H_5OH$	58.99	1.16E-09	9	500	5
$[(L^1)Dy(NO_3)_2(C_2H_5OH)_2](H_2O)$	203.11	1.77E-09	9	0	5
$[Dy(hmb)(NO_3)_2(DMF)_2]$	34	3.20E-06	9	1800	6
$[Dy(L^2)_2](CF_3SO_3)_3$	79	2.90E-08	10	1200	7
$[Dy(Hpaa)_2(H_2O)_4](Cl)_3$	179	1.99E-07	9	0	8
$[Dy(Hpaa)_2(NO_3)_2(MeOH)](NO_3)$	64	6.20E-07	9	2000	8
$[Dy(15C5)(H_2O)_4](ClO_4)_3(15C5)(H_2O)$	48.9/27.4	8.51E-11/3.27E-7	9	300	9
$[Dy(Phen)_2(NO_3)_3]$	101.02 /3.2	1.9E-11/4.5E-4	10	3500	10
$[Dy(ntbi)(NO_3)_3]_2{\cdot}3CH_3OH$	53.4	1.60E-12	10	1200	11
$[Dy(ntbi)_2]_5{\cdot}15Cl18H_2O$	39.8	1.60E-07	10	1200	11
$[DyC_{18}H_{22}N_6O_8]$	50	6.50E-07	10	1000	12
$[DyC_{18}H_{26}N_6O_8]$	34	2.51E-06	10	1000	12
$[Dy(L^3)(NO_3)(H_2O)](NO_3)_2$	64.1	3.70E-13	9	1500	13
$[DyY(tpcb)(H_2O)_4(NO_3)](NO_3)_2bpe$	55	9.81E-09	9	0	14
$[DyY(tpcb)(H_2O)_8(NO_3)_4](NO_3)_2{\cdot}2bpe2tpcb$	48	1.22E-09	9	400	14
$[Dy(2,3'\text{-}pcad)(NO_3)_2(CH_3OH)_2]$	56.11	2.90E-06	9	1200	15
$[Dy(2,3'\text{-}pcad)_2(H_2O)_3]_3Cl{\cdot}5H_2O$	72.4	3.00E-09	9	1200	15
$[Dy(2,3'\text{-}pcad)(NO_3)(H_2O)_4]NO_3{\cdot}H_2O$	24.95	5.50E-08	9	1200	15
fac-$[Dy(HL)_3]{\cdot}8H_2O$	19.5	7.00E-09	9	1000	16
mer-$[Dy(HL)_3]{\cdot}7H_2O$	34	1.60E-09	9	1000	16
$[Dy(Murex)_3]$	33	5.50E-10	9	1500	17
$[Dy(phen)(acac)_3]$	63.84	5.73E-06	10	0	18
$[Dy(tbpy)_2(NO_3)(DMF)]DMF$	22.61	9.77E-07	9	2000	19
$[Dy(H_2L^4)(NO_3)_3]{\cdot}2CH_3OH$	8.8 /32	2.4E-5/1.3E-7	9	1000	20
$[DyL^5(NO_3)_2]$	50	6.80E-07	10	1000	21
$[Dy(12\text{-}crown\text{-}4)(NO_3)_3]$	75.92	6.80E-11	10	500	22
$[Dy(HL^6)_3](DMF)$	270	1.3E-10	9	0	23
$[Dy(L^7)_3]CH_3OH$	13.7	1.20E-07	9	1000	24
$[Dy(L^7)_2(tmh)(CH_3OH)]{\cdot}CH_3OH{\cdot}H_2O$	95.7	3.40E-07	9	1000	24
$[Dy(L^7)_2(tta)(CH_3OH)]{\cdot}CH_3OH$	76	4.20E-08	9	1000	24
$[Dy(H_2TEG)(NO_3)_3][18\text{-}crown\text{-}6]$	28	2.49E-09	10	1000	25
$[Dy(H_2TEG)Cl_3][18\text{-}crown\text{-}6]$	54	1.44E-10	10	1500	25
$[Dy(Tppy)F(dioxane)](PF_6)$	621	1.48E-11	9	0	26
$[Dy(Tppy)F(pyridine)_2](PF_6)$	483	9.63E-11	9	0	26
$[Dy(L6\text{-}2H)(NO_3)2(DMF)_2](DMF)$	36	4.40E-06	9	1800	27
$[Dy(H_2DABPH)_2](NO_3)_3{\cdot}2.5H_2O$	32.4	N/A	10	1000	28
$[Dy(H_2DABPH)(HDABPH)](NO_3)_2{\cdot}EtOH{\cdot}4H_2O$	<19	N/A	10	1000	28
$[Dy(H_5L^8)(NO_3)_2(CH_3OH)_2]{\cdot}4CH_3OH$	28.5	2.02E-06	9	800	29
$[Dy(12\text{-}C\text{-}4)(NO_3)_3]$	68	2.07E-10	9	1000	30
$[Dy(18\text{-}C\text{-}6)(NO_3)_2]ClO_4$	63	1.02E-08	9	1000	30
$[Dy(18\text{-}C\text{-}6)(NO_3)_2]BPh_4$	43	1.37E-06	9	1000	30
$[Dy(H_4daps)(H_2O)_3(NO_3)](NO_3)_2(H_2O)$	32.7	1.82E-06	9	2000	31
$[Dy(H_3daps)(H_2O)_2(NO_3)](NO_3)(MeOH)$	23.8	9.14E-05	9	2000	31
$[Dy(nma)(NO_3)_2(DMSO)]CH_3OH$	67	1.68E-07	9	2000	32
$[Dy(nma)_2]{\cdot}ClO_4{\cdot}0.5CH_3OH$	16 /47	1E-5/4.6E-6	9	2000	32
$[Dy(HL^9)_2(NO_3)_3]$	23.8/22.7	2.47E-6/3.6E-7	10	2000	33

$[Dy(NO_3)_3(5BrsalanH)2(H_2O)]MeCN$	38.8	2.50E-06	9	1000	34

HL^1 = N^3-(2-pyridoyl)-4-pyridinecarboxamidrazone, Hhmb = N'-(2-hydroxy3-methoxybenzylidene)benzohydrazide, L^2 = 2,6- diacetylpyridinebis(2'-pyridylhydrazone), Hpaa = N-(2-pyridyl)-ketoacetamide, 15C5 = crown ether, Phen = 1,10-phenanthroline, ntbi = tris(benzimidazol-2-ylmethyl)amine, $L^{3=}$ {(3,12-bis(2-pyridylmethyl)-3,12,18-triaza-6,9-dioxabicyclo-[12.3.1]octadeca-1,14,16-triene), bpe = 1,2-bis(4-pyridyl)ethane, tpcb = tetrakis(4-pyridyl)cyclobutane, 2,3'-Hpcad = N^3-(2-pyridoyl)-3-pyridinecarboxamidrazone, Murex = 2,6-dioxo-5-[(2,4,6-trioxo-5-hexahydropyrimidinylidene)amino]-3H-pyrimidin-4-olate, tbpy = 6-(tetrazol-5-yl)-2,2'-bipyridine, H_2L^4 = N,N' ,N''-trimethyl-N,N''-bis(2-hydroxy-3-methoxy5-methylbenzyl) diethylene triamine, L^5 = N,N'-bis-pyridin-2-yl-methelene-1,8-diamino-3,6-dioxaoctane, H_2L^6 = 2-hydroxy-N'-[(E)-(2-hydroxy-3-methoxyphenyl)methylidene]benzhydrazide, HL^7 = 2-(tetrazol-5-yl)-1,10-phenanthroline, tta = 2-thenoyltrifluoroacetonate, tmh = 2,2,6,6-tetramethylheptanoate, H_2TEG = triethylene glycol, Tppy = tris(3-(2-pyridyl)pyrazolyl)hydroborate, L6-2H = derivative of (1Z,2E,N'E)-N'-(2-hydroxy-3-methoxybenzylidene)-2-(hydroxyimino)propanehydrazonic acid, H2DABPH = 2,6-diacetylpyridinebis(benzoic acid) hydrazine, H_6L^8 = N'-((1,8-dihydroxynaphthalene-2,7-diyl)bis(methanylylidene))bis(2-hydroxybenzohydrazide), H_4daps = 2,6-bis(1-salicyloylhydrazonoethyl)pyridine, Hnma = N-(2-(8-hydroxylquinolinyl)methane(2-(4-imidazolyl)ethanamine, HL^9 = 2-methoxy-6-[(E)-phenyliminomethyl]phenol, 5BrsalanH = N-(5-bromosalicylidene)aniline

Table S7. CASSCF+RASSI-SO computed relative energies of the eight low lying Kramers Doublets along with g tensors and deviations from the principal magnetization axis with respect to the first KD for complex **1**.

E (K)	g_{xx}	g_{yy}	g_{zz}	Angle (°)
0.0	0.006	0.012	19.837	
184.9	0.212	0.228	16.800	0.0
381.0	0.468	0.583	13.380	0.0
526.6	5.213	5.565	8.350	0.1
626.6	2.259	2.519	14.626	90.0
668.3	0.666	0.736	12.369	89.9
695.2	0.329	1.773	13.286	89.9
808.0	0.071	0.120	19.587	89.8

Table S8. CASSCF+RASSI-SO computed relative energies of the eight low lying Kramers Doublets along with g tensors and deviations from the principal magnetization axis with respect to the first KD for Models **1-9** respectively.

Model-1 (changing axial F^- for OH^-)				
E (K)	**g_{xx}**	**g_{yy}**	**g_{zz}**	**Angle (°)**
0.0	0.009	0.033	19.687	
143.3	0.560	0.600	16.390	0.0
270.1	0.114	0.815	13.060	0.0
370.8	4.751	5.432	8.975	0.0
466.0	0.190	5.168	10.759	90.0
514.5	1.797	4.390	13.539	90.0
559.0	0.121	0.634	18.793	90.0
646.6	0.038	0.075	19.572	90.0

Model-2 (changing axial F^- for CHO_2^-)				
E (K)	**g_{xx}**	**g_{yy}**	**g_{zz}**	**Angle (°)**
0.0	3.863	6.423	11.446	
33.5	2.606	4.495	8.571	138.8
48.2	7.726	5.582	0.303	18.6
87.2	6.437	5.628	2.243	142.0
175.1	0.592	1.686	14.752	36.1
202.6	10.559	6.149	0.484	51.5
226.5	2.782	4.545	11.478	119.9
293.4	0.159	0.503	18.459	68.6

Model-3 (changing axial F for $tBuCO_2^-$)				
E (K)	**g_{xx}**	**g_{yy}**	**g_{zz}**	**Angle (°)**
0.0	3.763	5.910	11.588	
30.2	1.586	3.746	12.202	34.0
48.2	7.813	6.799	0.816	60.0
94.0	8.380	5.821	1.074	23.9
171.8	0.817	2.313	13.379	37.3
193.5	9.460	7.802	0.561	63.7
222.4	4.143	5.557	9.887	57.7
281.3	0.358	0.996	18.055	63.8

Model-4 (changing axial F for $CF_3CO_2^-$)				
E (K)	**g_{xx}**	**g_{yy}**	**g_{zz}**	**Angle (°)**
0.0	11.499	6.983	1.153	
20.1	0.373	6.293	12.510	104.2
57.8	9.004	7.216	2.380	21.3
110.2	8.449	6.692	1.502	80.8
178.6	1.440	2.288	11.962	70.0
200.4	9.626	8.015	0.414	49.4
239.1	4.458	4.822	7.957	136.1
283.2	0.948	3.344	16.296	92.7

Model-5 (changing axial F for $CH_3CH_2CH_2O^-$)				
E (K)	**g_{xx}**	**g_{yy}**	**g_{zz}**	**Angle (°)**
0.0	0.010	0.034	19.668	
135.8	0.567	0.586	16.400	0.5
261.4	0.069	0.766	13.052	3.5
361.3	4.876	5.492	8.954	14.2
457.1	0.582	5.212	10.010	92.5
502.0	1.983	5.061	13.061	89.1
549.8	0.126	0.563	18.844	88.7
630.8	0.038	0.088	19.537	89.9

Model-6 (changing axial F for $tBuCH_2CH_2O^-$)				
E (K)	**g_{xx}**	**g_{yy}**	**g_{zz}**	**Angle (°)**
0.0	0.009	0.031	19.686	
140.4	0.528	0.545	16.441	0.6
269.8	0.026	0.660	13.109	3.3
372.4	4.870	5.361	9.035	14.1
469.3	9.651	5.345	0.792	81.6
514.2	2.100	5.355	12.818	90.8
563.9	0.114	0.516	18.890	88.7
641.3	0.038	0.088	19.545	90.1

Model-7 (adding ortho F group to the cage ligand)				
E (K)	**g_{xx}**	**g_{yy}**	**g_{zz}**	**Angle (°)**
0.0	0.002	0.004	19.882	
241.0	0.122	0.126	16.913	0.0
469.8	0.078	0.163	13.805	0.0
645.4	3.440	3.533	10.097	0.0
765.1	9.011	5.784	1.350	89.8
812.3	1.343	5.539	13.147	89.8
855.9	0.401	1.541	18.327	90.0
933.5	0.043	0.258	19.594	89.8

Model-8 (adding ortho CN group to the cage ligand)				
E (K)	**g_{xx}**	**g_{yy}**	**g_{zz}**	**Angle (°)**
0.0	0.003	0.007	19.865	
211.5	0.182	0.189	16.857	0.0
421.0	0.121	0.223	13.546	0.0
575.5	5.135	5.237	8.760	0.0
683.0	1.612	3.189	12.868	89.9
719.0	0.075	2.662	14.869	89.8
764.7	0.134	0.915	18.093	90.0
844.3	0.106	0.242	19.542	90.0

Model-9 (adding para NO_2 group to the cage ligand)				
E (K)	**g_{xx}**	**g_{yy}**	**g_{zz}**	**Angle (°)**
0.0	0.003	0.007	19.861	
203.4	0.172	0.178	16.865	0.0
412.6	0.132	0.235	13.595	0.0
570.5	4.768	4.838	9.048	0.0
680.4	1.745	3.702	11.834	89.9
716.8	0.258	3.208	14.464	89.8
755.9	0.211	1.185	17.633	89.8
842.6	0.110	0.252	19.531	89.8

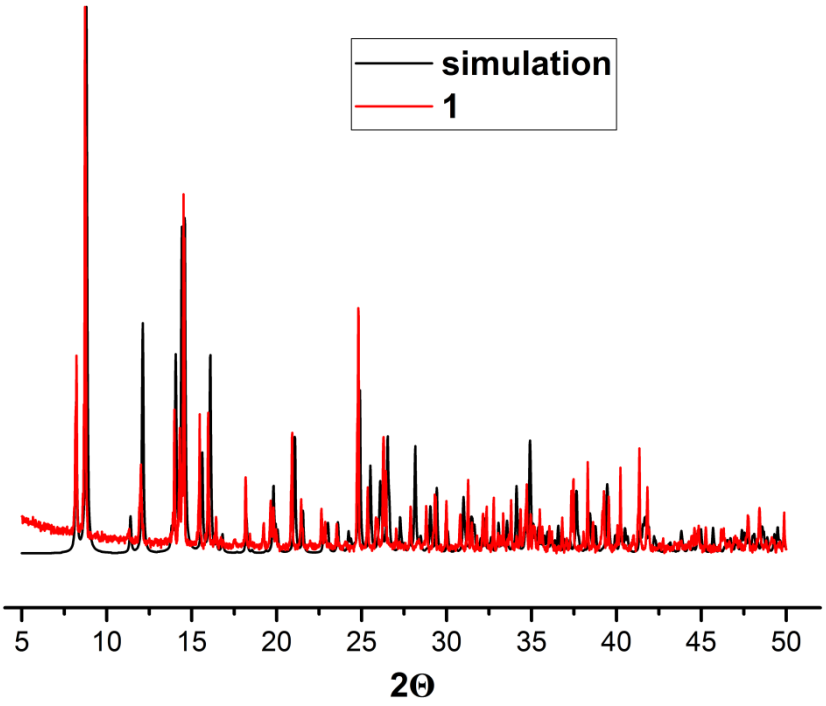

Fig. S3 The powder X-ray diffraction pattern of **1.** The black line represents the simulated powder X-ray diffraction pattern generated from single-crystal data collected at 150 K, and the red line represents the experimental data measured at ambient temperature.

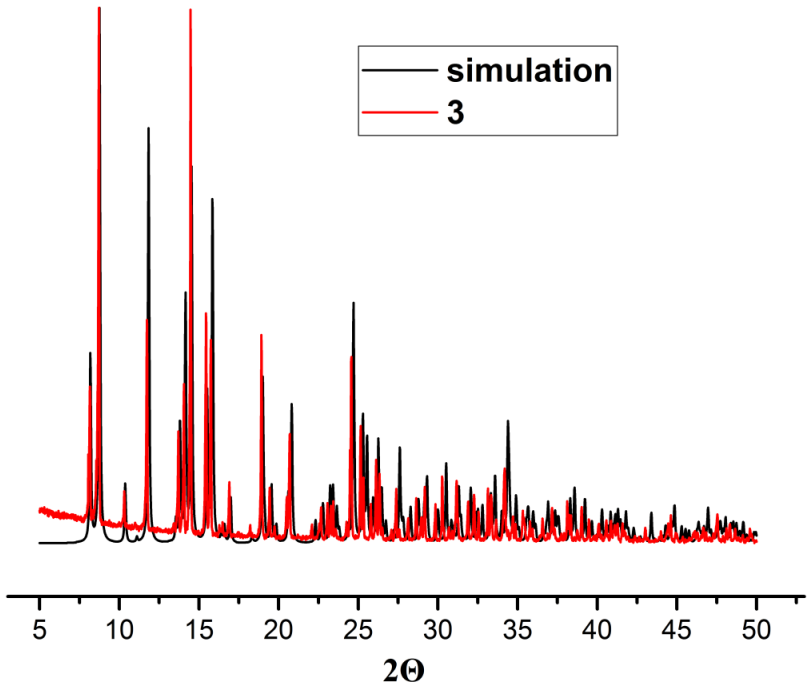

Fig. S4 The powder X-ray diffraction pattern of **3.** The black line represents the simulated powder X-ray diffraction pattern generated from single-crystal data collected at 150 K, and the red line represents the experimental data measured at ambient temperature.

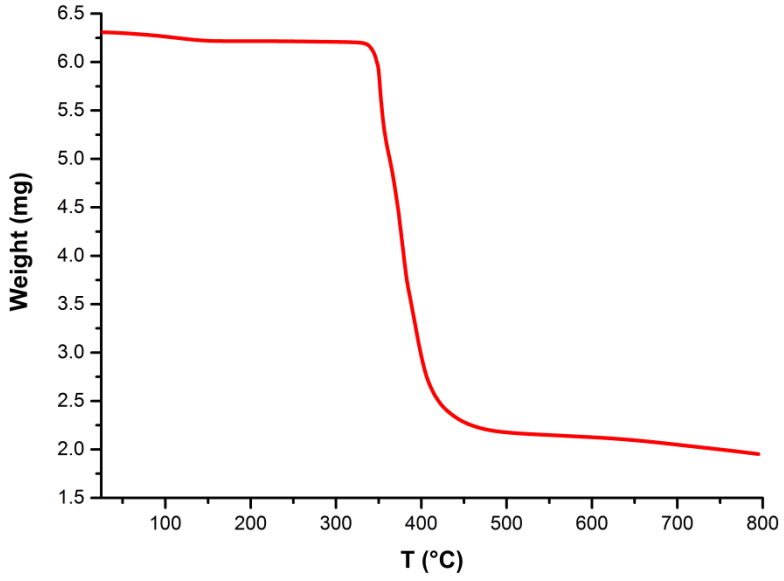

Fig. S5 Thermogravimetric analysis for **1** under an argon atmosphere (10 K min^{-1}).

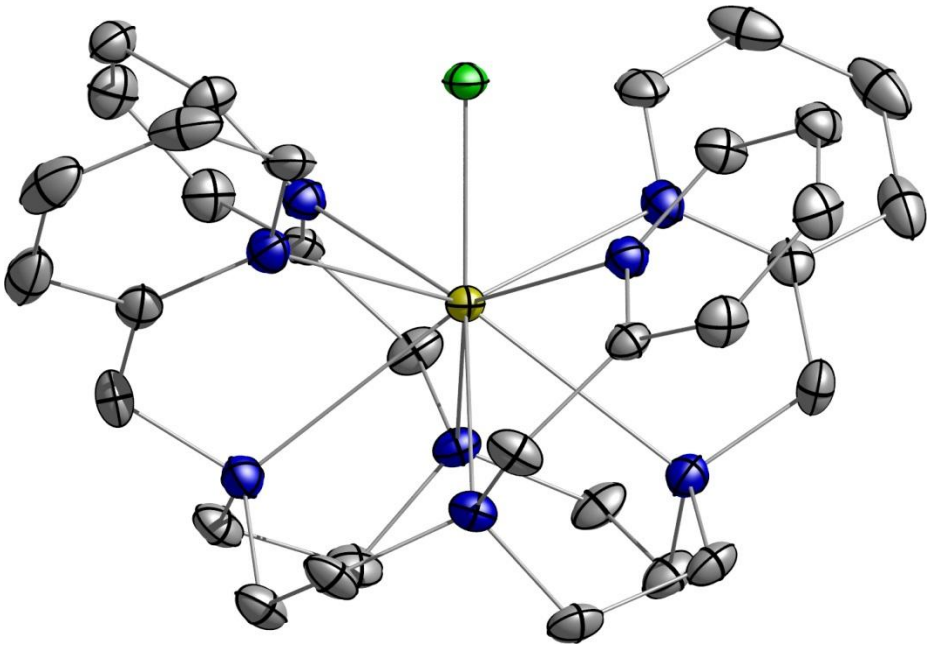

Fig. S6 The displacement ellipsoids for **1** are drawn at 50% probability level. Hydrogen atoms, the co-crystallised water molecule and counter-ions are omitted for clarity. Dy, gold; N, blue; F, green; C, grey.

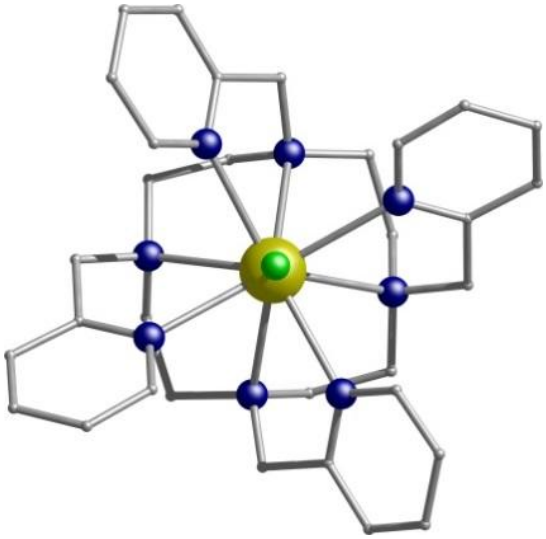

Fig. S7 The structure of **1.** The polydentate ligand is able to encapsulate and stabilise the dysprosium centre in a $\{N_8\}$ coordination environment with the Dy-N bond distances falling in two categories: i) those between Dy-N_{py} that are shorter falling in the 2.531(3)-2.541(3) range and ii) those between Dy-N_{am} that are longer in the 2.669(3)-2.689(3) Å range. (Table S3, ESI). Dy, gold; N, dark blue; F, green; carbon, grey.

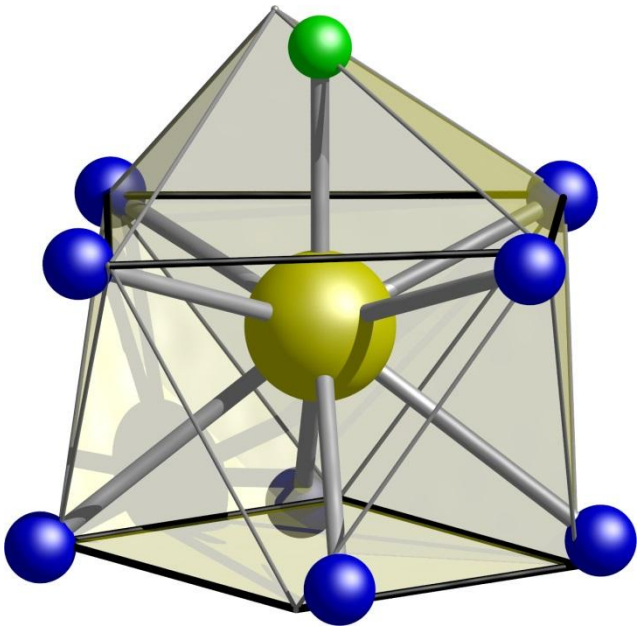

Fig. S8 Comparison of the calculated (with SHAPE[4]) and experimental muffin coordination sphere for the Dy(III) ion in complex **1** . The geometry of {DyN_8} core is very close to an ideal square antiprismatic geometry (*pseudo* D_{4d} symmetry) as shown by the SHAPE analysis (1.411) (Table S5). Dy, gold; N, dark blue; F, green.

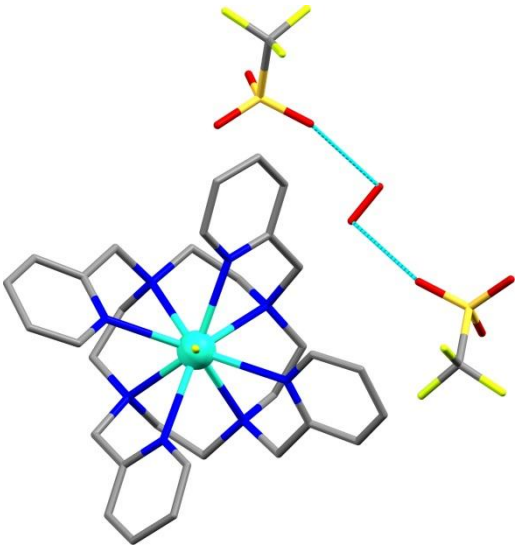

Fig. S9 Intermolecular hydrogen bonding in **1**. Hydrogen atoms are omitted for clarity. The co-crystallised water molecule shows some disorder. Dy, cyan; N, dark blue; F, green; S, yellow; O, red.

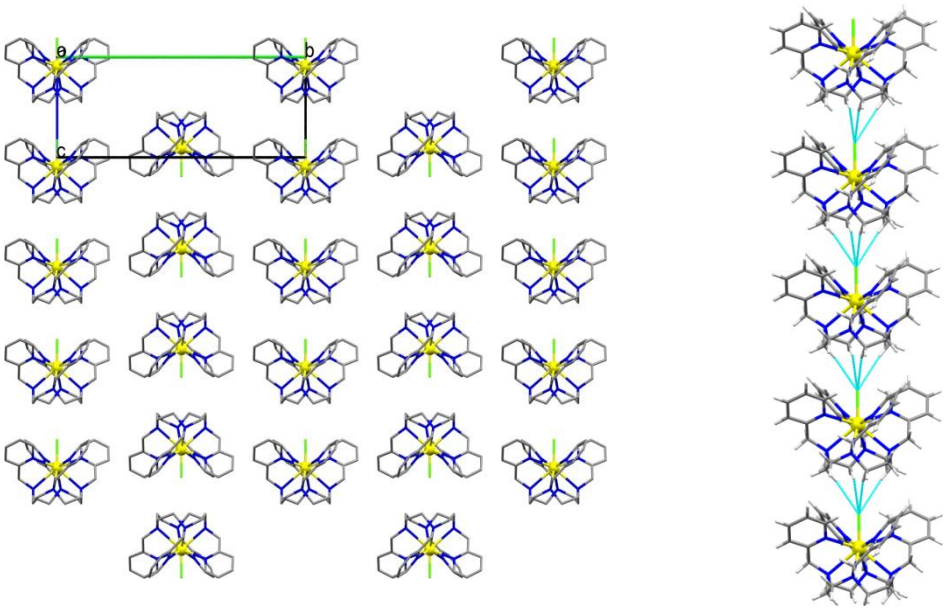

Fig. S10 (Left) The columnar crystal packing of **1** looking down the *a* axis. (Right) The C-H···F intermolecular interactions between neighboring molecules of **1**. Hydrogen atoms are omitted for clarity, except for the hydrogens atoms that are emphasized in the C-H···F interactions. The co-crystallised water molecule and counter-ions are omitted for clarity. Dy, gold; N, dark blue; F, green.

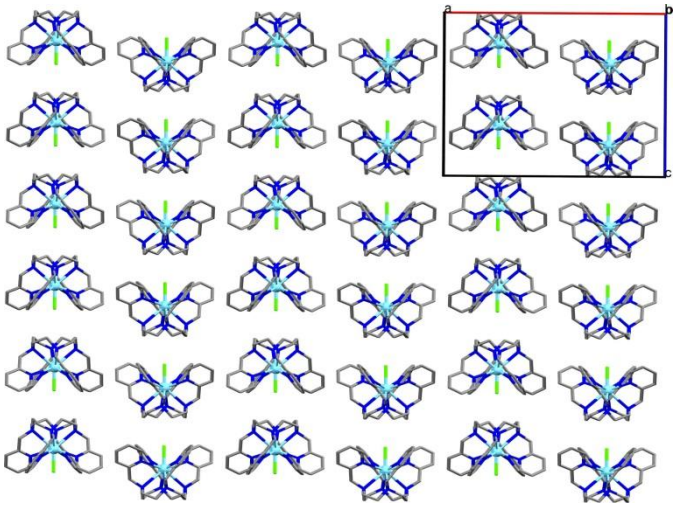

Fig. S11 The columnar crystal packing of $[La^{III}LF](CF_3SO_3)_2 \cdot H_2O$ (**2**) looking down the *b* axis. Hydrogen atoms are omitted for clarity. The co-crystallised water molecule and counter-ions are omitted for clarity. La, sky blue; N, dark blue; F, green.

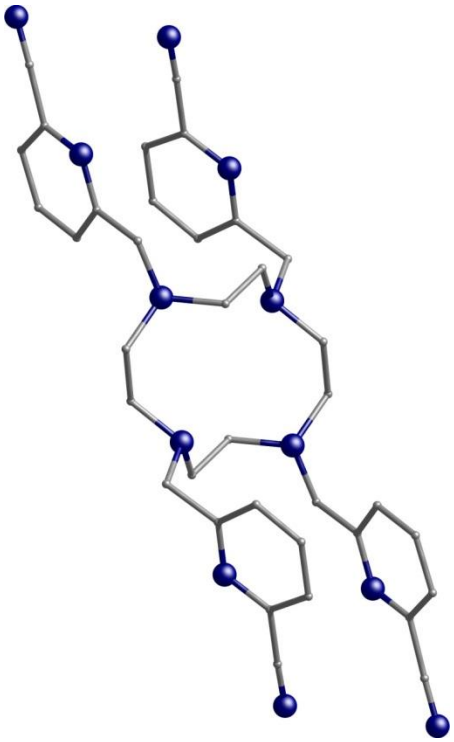

Fig. S12 The crystal structure of the new ligand, **4**, where the electron withdrawing group, CN, has been included in the *ortho* position of the rings**.**

Magnetic Properties

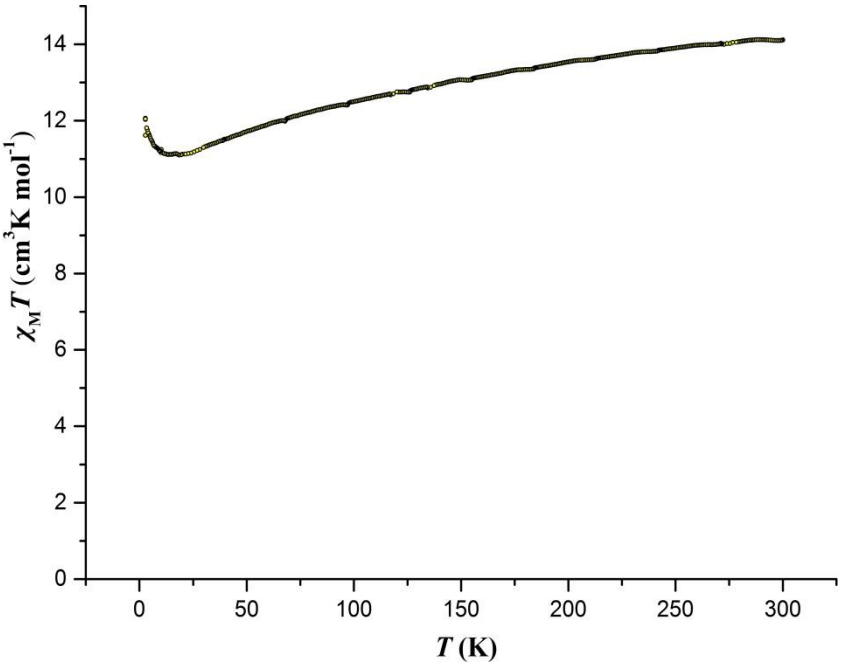

Fig. S13 $\chi_M T$ vs. T data for **1** in a field of 1000 Oe from 300 – 2.8 K.

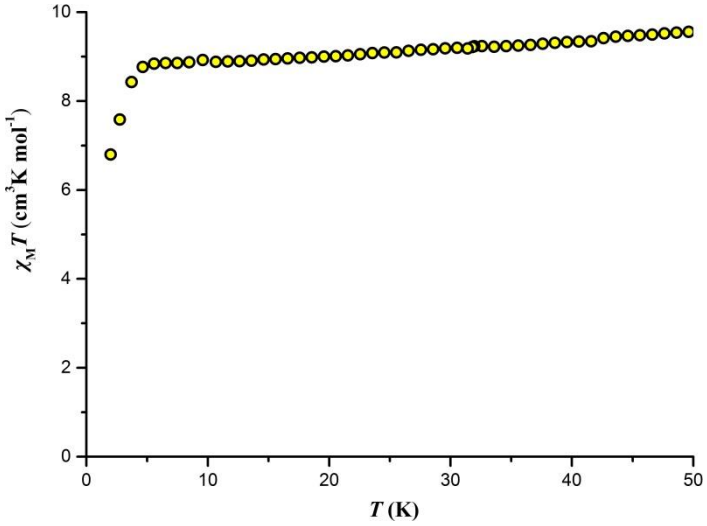

Fig. S14 $\chi_M T$ vs. T data for **3** in a field of 1000 Oe from 50 – 2.8 K.

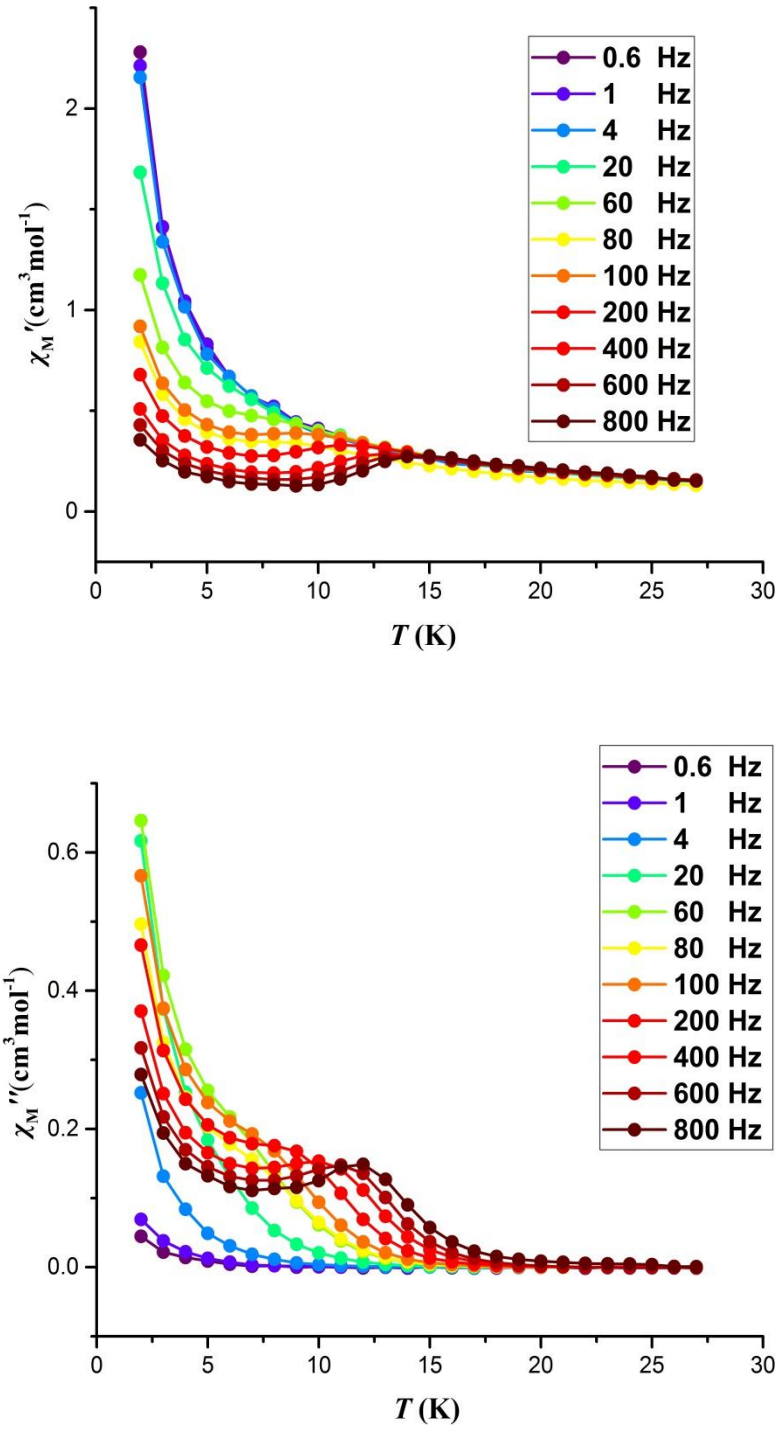

Fig. S15 Temperature dependence of the in-phase, χ'_M (upper), and out-of-phase, χ''_M (lower) susceptibility, in zero dc field, for **1** with ac frequencies of 0.6–800 Hz.

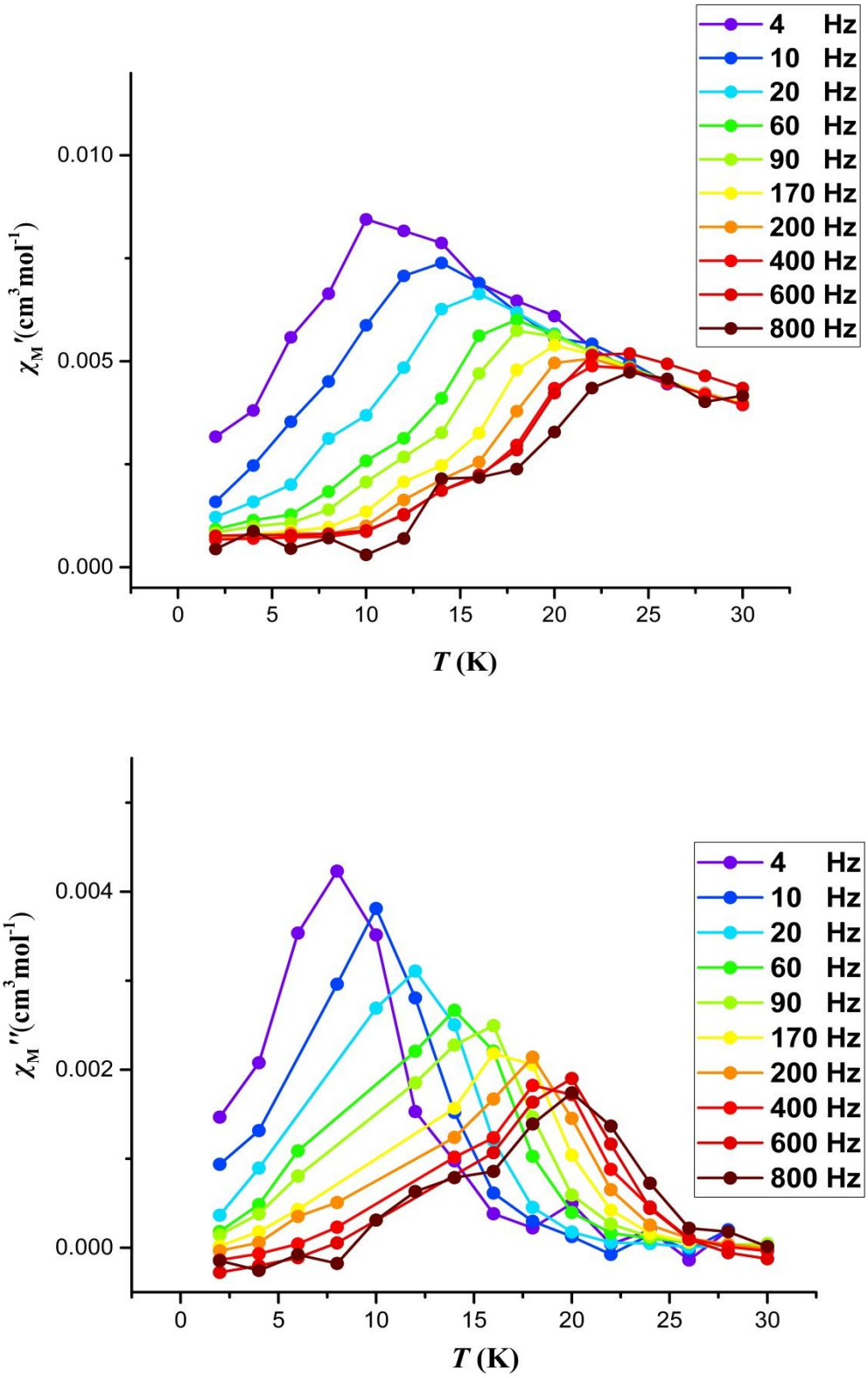

Fig. S16 Temperature dependence of the in-phase, χ'_M (upper), and out-of-phase, χ''_M (lower) susceptibility, in zero dc field, for the doped sample **3** with ac frequencies of 4–800 Hz.

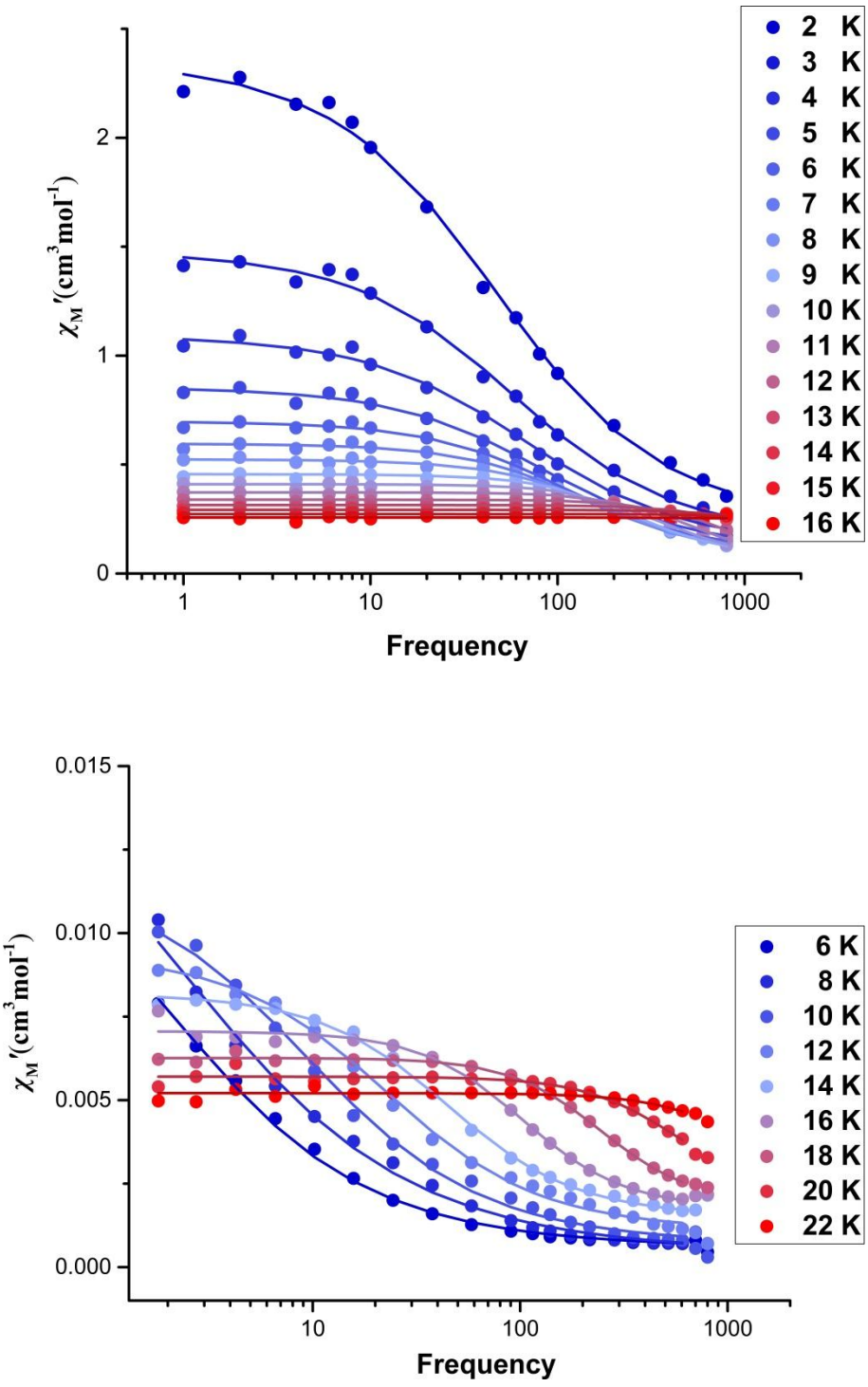

Fig. S17 Frequency dependence of the in-phase susceptibility for **1** (upper) and **3** (lower), in zero dc field. The solid lines correspond to the best fit.

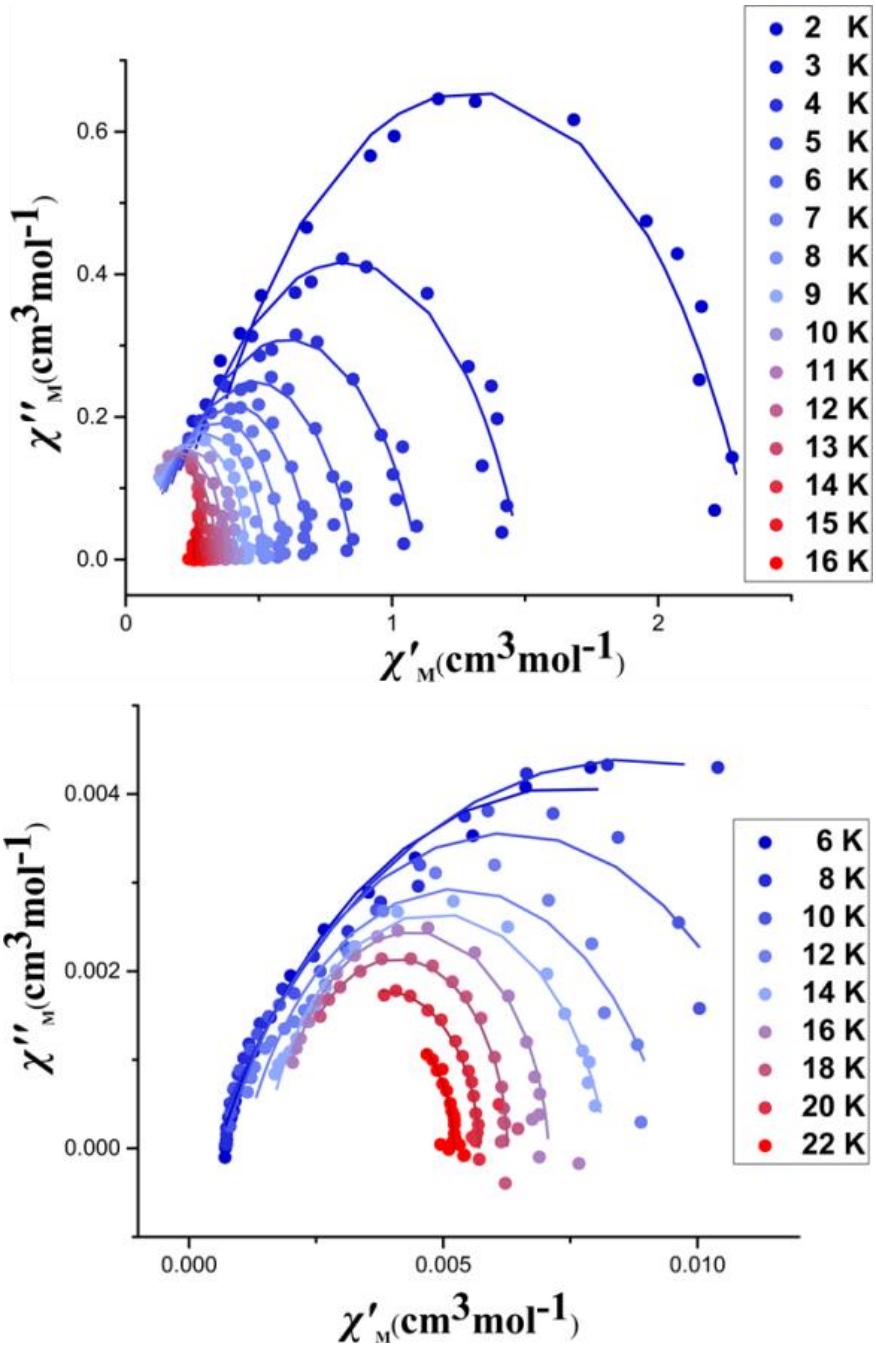

Fig. S18 χ''_M vs χ'_M plot of the AC magnetic susceptibility of **1** (upper) and **3** (lower), in zero dc field. The solid lines correspond to the best fit to Debye's law.

Fitting of the relaxation times

The plot of the relaxation times τ^{-1} versus T for **1, 3** and **1@1600** were analysed with multiple relaxation processes using equation 1.[35]

$$\tau^{-1} = \tau_{QTM}^{-1} + CT^{n} + \tau_{0}^{-1} \exp(-U_{eff}/T) \qquad (1)$$

where τ_{QTM}^{-1} accounts for the temperature independent quantum tunnelling of magnetization, CT^{n} represents the Raman relaxation process (typically n = 4, 5, 7, 9) and $\tau_{0}^{-1} \exp(-U_{eff}/T)$ accounts for the Orbach process.

Table S9. Parameters obtained from the fitting of the relaxation times for **1, 3** and **1@1600 Oe**.

Complex	U_{eff} (K)	τ_0 (s)	τ_{QTM} (s)	C (K^{-n} s^{-1})	n
1	116	0.40×10^{-7}	0.02	$8.1\ 10^{-3}$	5.3
3	291	0.45×10^{-9}	-	$4.5\ 10^{-5}$	6
1@1600 Oe	178	0.60×10^{-9}	-	$2.2\ 10^{-3}$	5.5

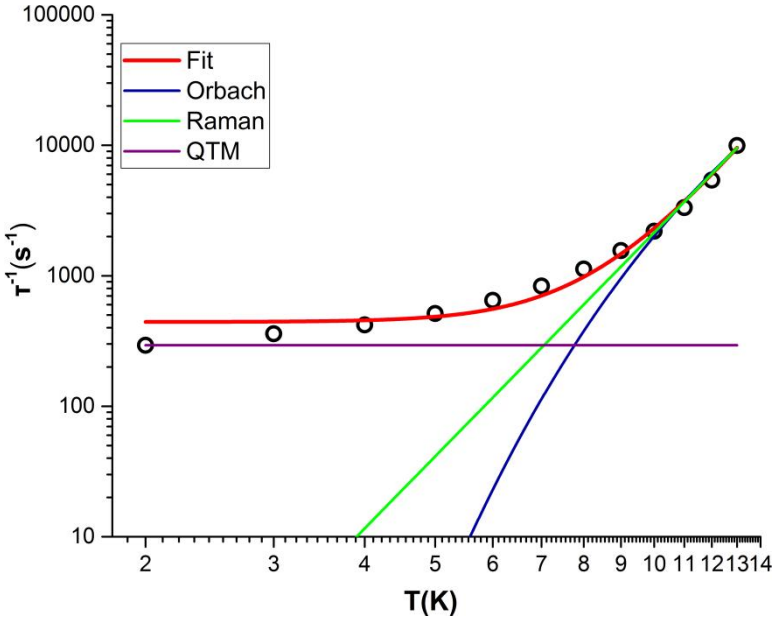

Fig. S19 Log-Log plot of the relaxation times, τ^{-1} versus T for **1**. The data were analysed using the equation: $\tau^{-1} = \tau_{QTM}^{-1} + CT^n + \tau_0^{-1} \exp(-U_{eff}/T)$. The best fit (red line) gives n = 5.3, C = 8.1 10^{-3} K^{-n} s^{-1}, τ_{QTM} = 0.02 s , τ_0 = 0.40 x 10^{-7} s and U_{eff} = 116 K.[36]

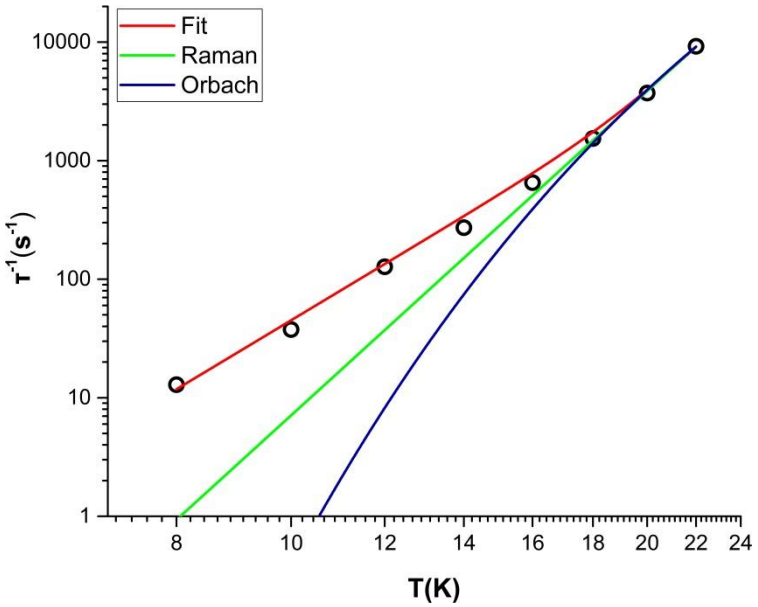

Fig. S20 Log-Log plot of the relaxation times, τ^{-1} versus T for **3**. The data were analysed using the equation: $\tau^{-1} = CT^n + \tau_0^{-1} \exp(-U_{eff}/T)$. The best fit (red line) gives n = 6, C = 4.5 10^{-5} K^{-n} s^{-1}, τ_0 = 0.45 x 10^{-9} s, and U_{eff}= 291 K.[36]

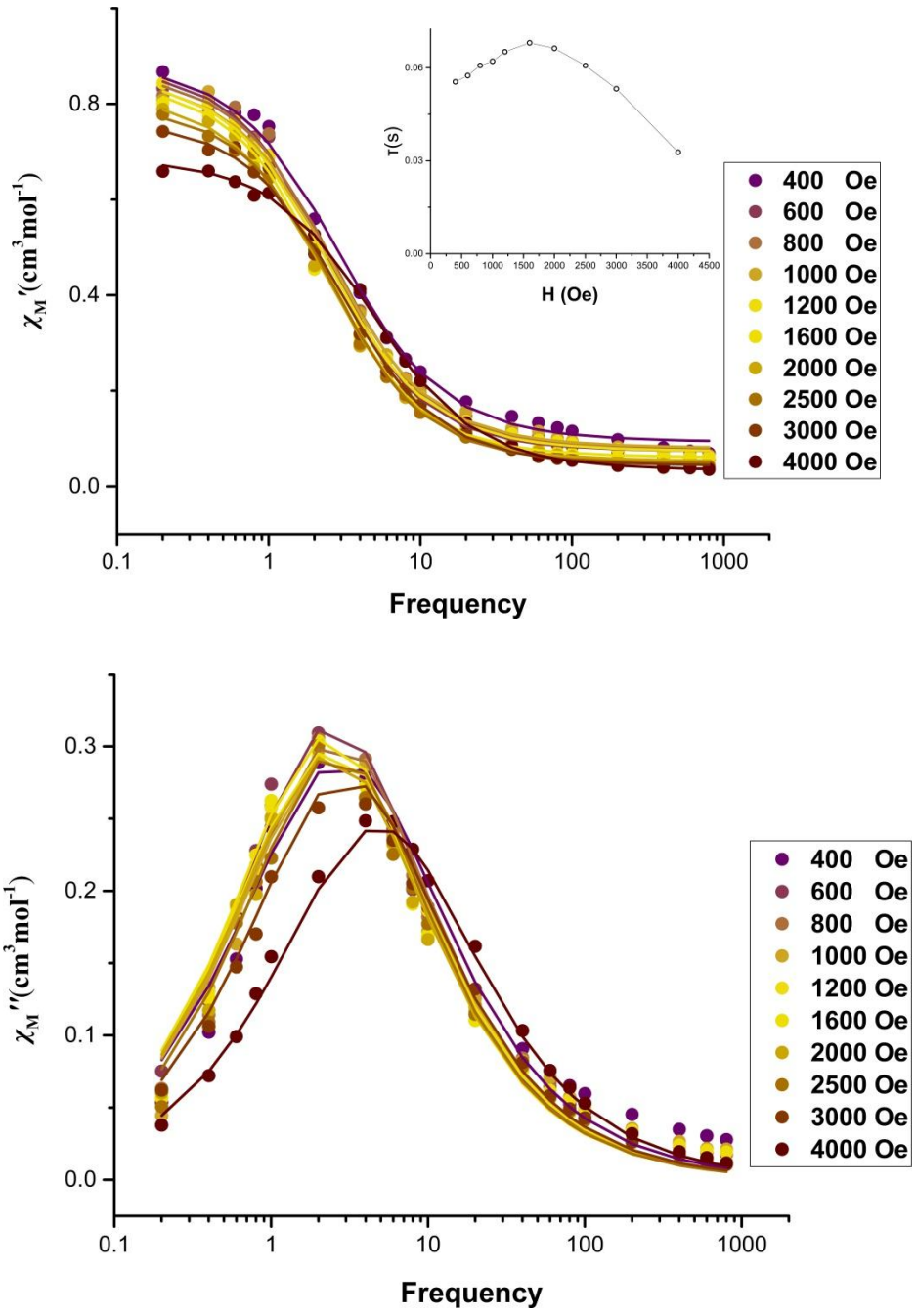

Fig. S21 Frequency dependence of the in-phase (upper) and out-of-phase (lower) susceptibility at 5 K measured at different dc fields for complex **1**. The solid lines correspond to the best fit. (Upper Inset) Relaxation times (τ) as a function of the applied field (Oe) for **1**, showing the optimum dc field as 1600 Oe.

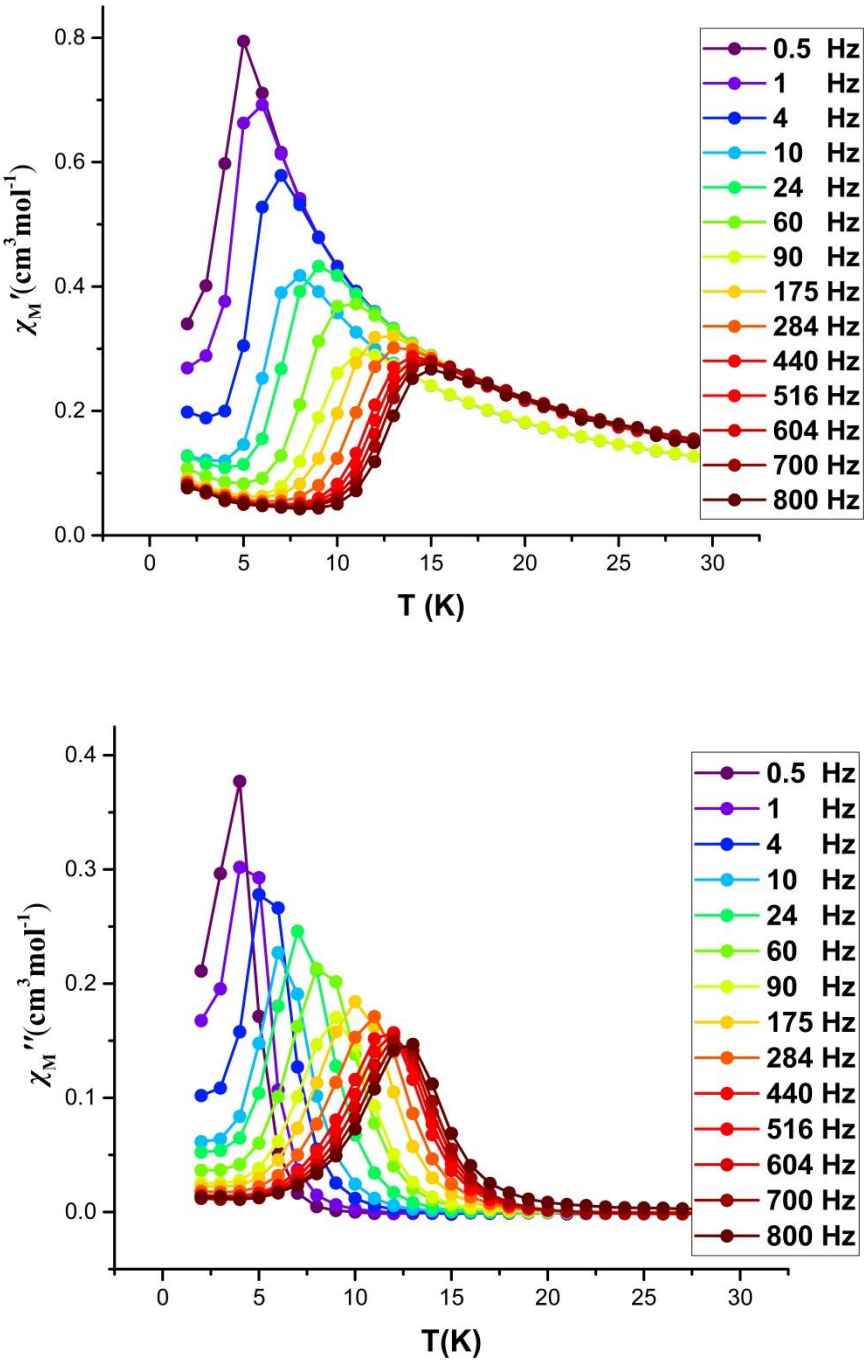

Fig. S22 Temperature dependence of the in-phase, χ'_M (upper), and out-of-phase, χ''_M (lower) susceptibility, measured in a 1600 Oe dc field, for **1** with ac frequencies of 0.5−800 Hz.

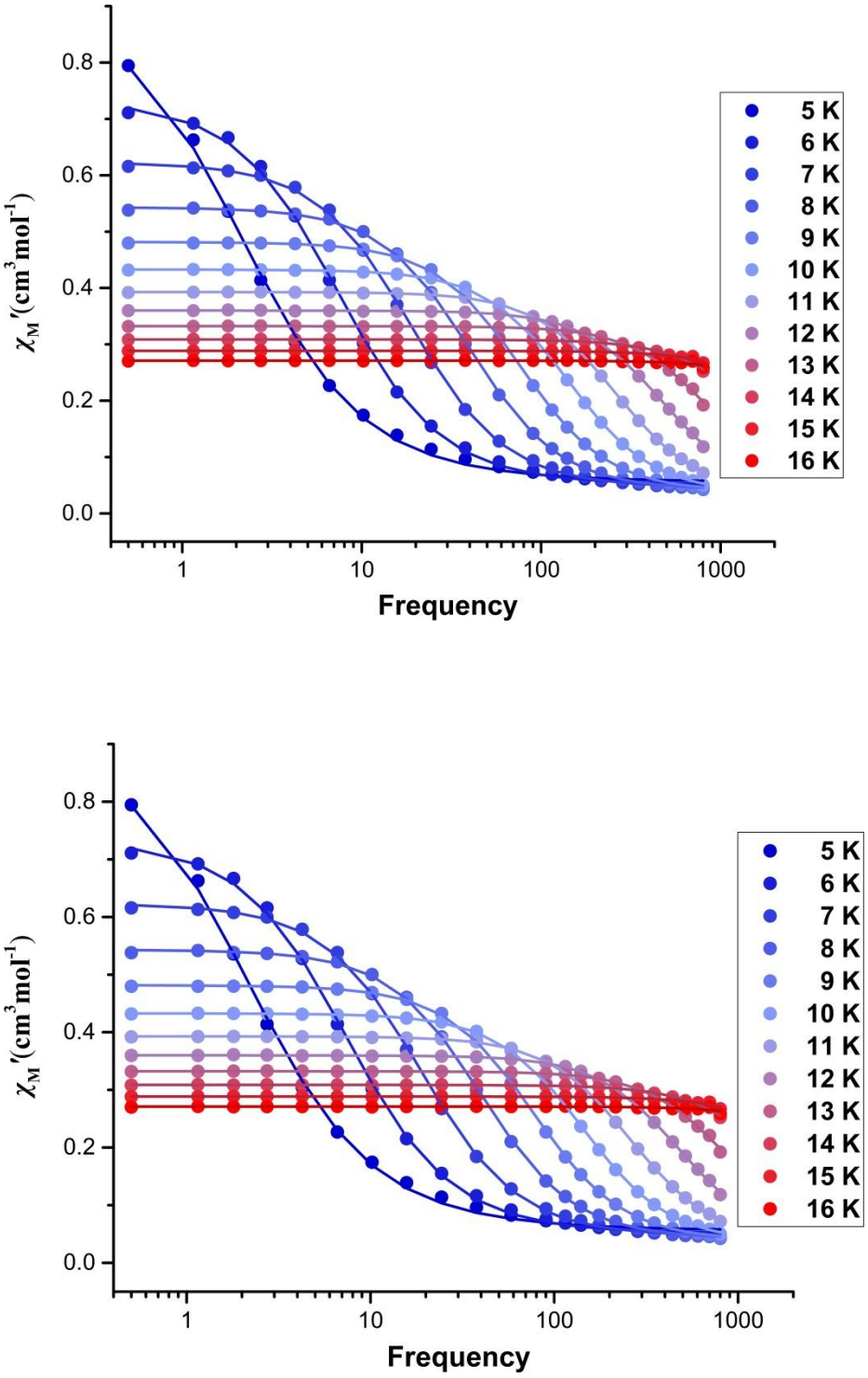

Fig. S23 Frequency dependence of the in-phase (upper) and out-of-phase (lower) susceptibility for complex **1**, in a 1600 Oe dc field. The solid lines correspond to the best fit.

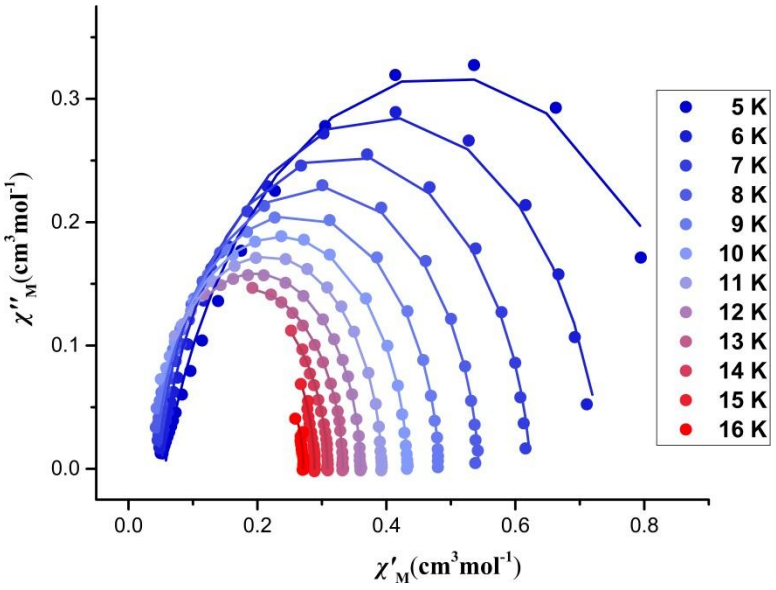

Fig. S24 χ''_M vs χ'_M plot of the AC magnetic susceptibility of **1**, measured in a 1600 Oe dc field. The solid lines correspond to the best fit to Debye's law.

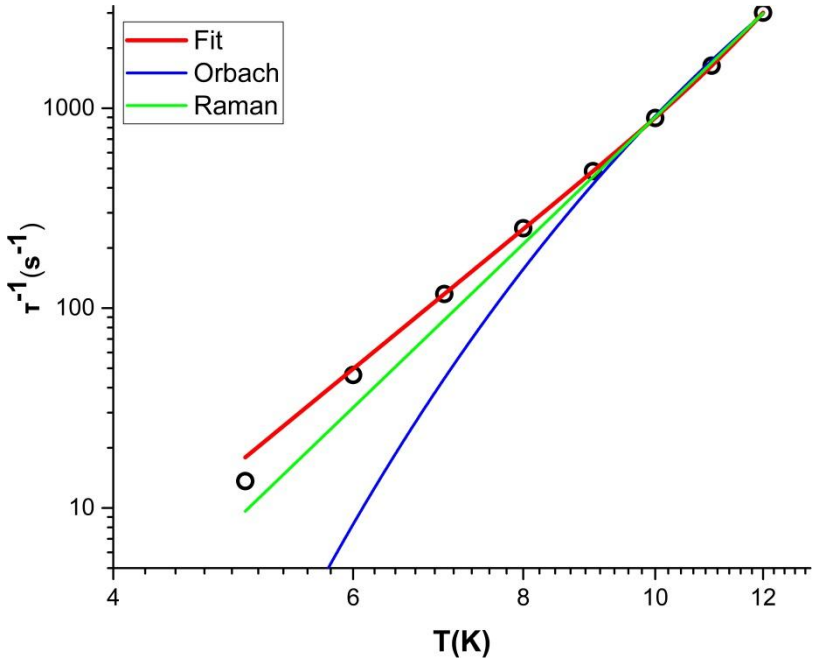

Fig. S25 Log-Log plot of the relaxation times, τ^{-1} versus T for **1** in a 1600 Oe dc field. The data were analysed by equation: $\tau^{-1} = CT^n + \tau_0^{-1} \exp(-U_{eff}/T)$. The best fit (red line) gives n= 5.5, C= 2.2 10^{-3} K^{-n} s^{-1}, $\tau_0 = 0.60 \times 10^{-9}$ s, and U_{eff} = 178 K.[36]

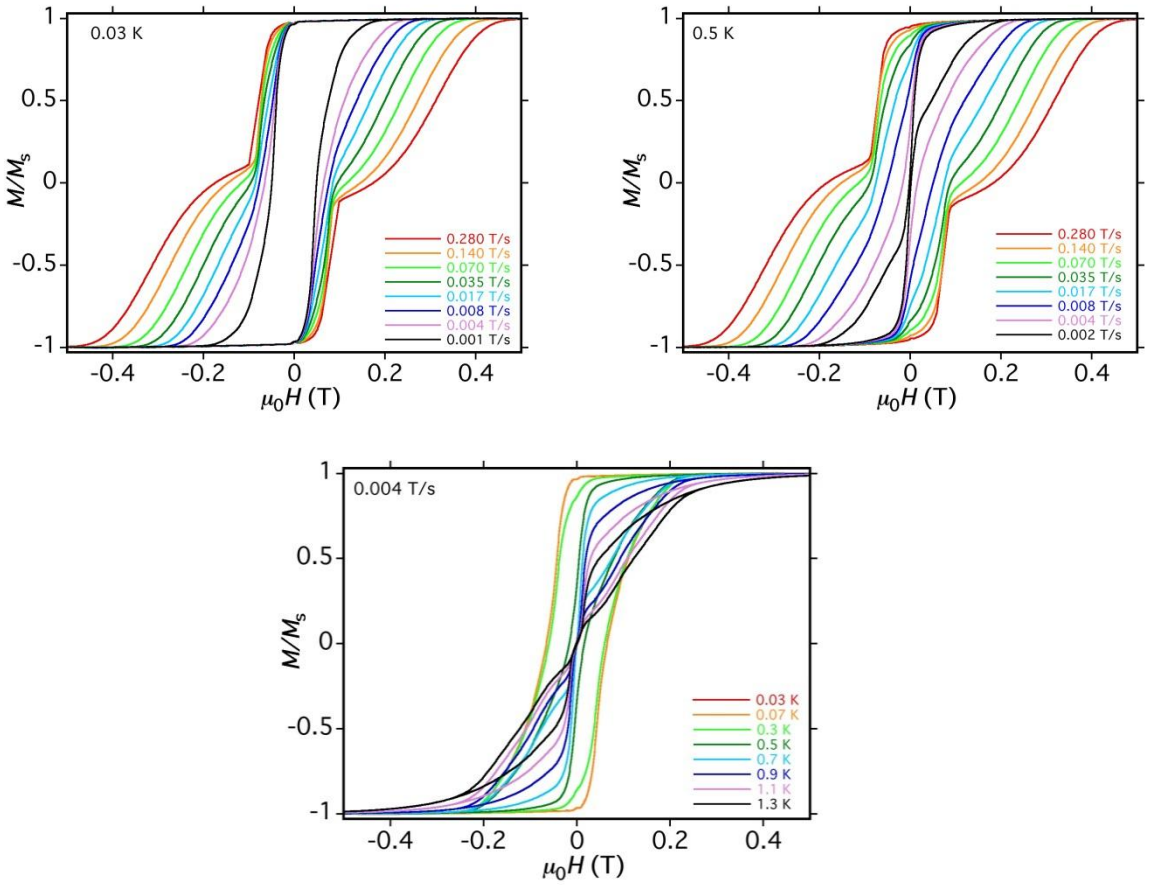

Fig. S26 Field dependence of the normalized magnetization of **1** obtained at various temperatures (upper) and field sweep rates (lower).

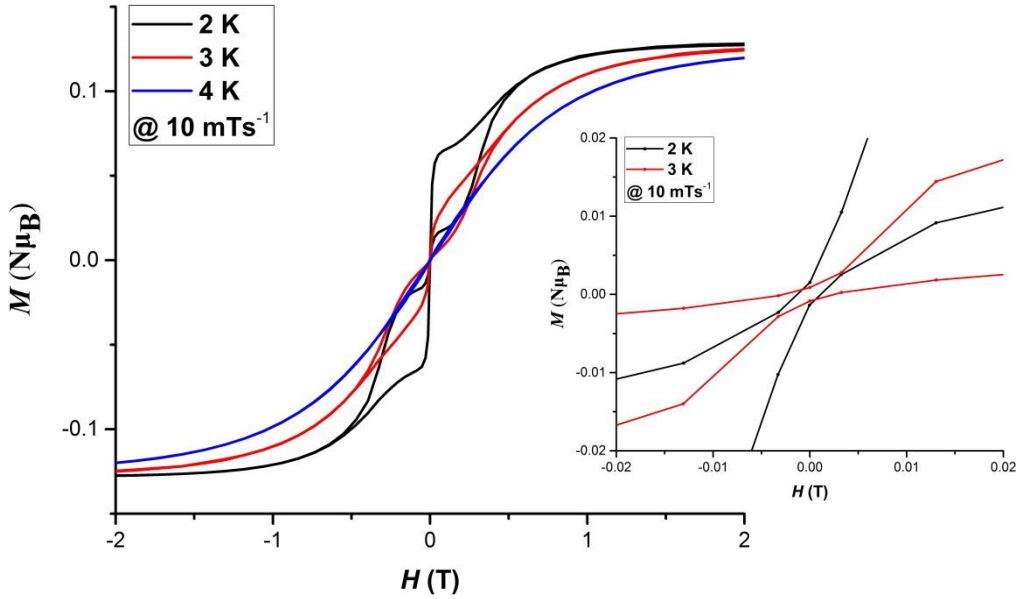

Fig. S27 Powder magnetic hysteresis measurements for **3** at 2-4 K with an average sweep rate of 10 mTs^{-1}.

Computational Details:

All the *ab initio* calculations have been performed using MOLCAS 8.0 code. The employed basis sets are given below:

C.ANO-RCC...3s2p.,
N.ANO-RCC...4s3p2d1f.,
O.ANO-RCC...3s2p1d.,
F.ANO-RCC...4s3p2d1f.,
S.ANO-RCC...4s3p1d.,
H.ANO-RCC...2s.,
Dy.ANO-RCC...8s7p5d3f2g1h..

For the $4f^9$ electronic configuration of Dy(III), the $^6H_{15/2}$ multiplet is expected to be the ground state. First, we have generated the guess orbitals and have selected seven Dy(III) based starting orbitals to perform the CASSCF calculations. CASSCF calculations have been performed using nine electrons in the seven active orbitals, with an active space of CAS(9,7). Using this active space, 21 sextets have been computed using the configuration interaction (CI) procedure. Then we have performed RASSI-SO module to compute the spin-orbit coupled states. After computing these SO states, we have performed the SINGLE_ANISO code to extract the corresponding g-tensors. Here we have computed the g-tensors for the eight low-lying Kramers Doublets. The Cholesky decomposition for two electron integrals is employed throughout in the calculations to reduce the disk space.[37]

In Silico Modelling: We have performed selective optimization for the model complexes, where we have used the experimental structural parameters and optimized selectively the additionally added functional group. For this, we have performed calculations in the Gaussian 09 program suite[38] using the hybrid B3LYP functional.[39] We have replaced Dy(III) ion with La(III) ion and treated by ECP SDD basis set.[40] For all other elements we have used the 6-31G basis set.[41] We have used same methodology to perform frequency calculation for complex **1** on the X-Ray reported structure.

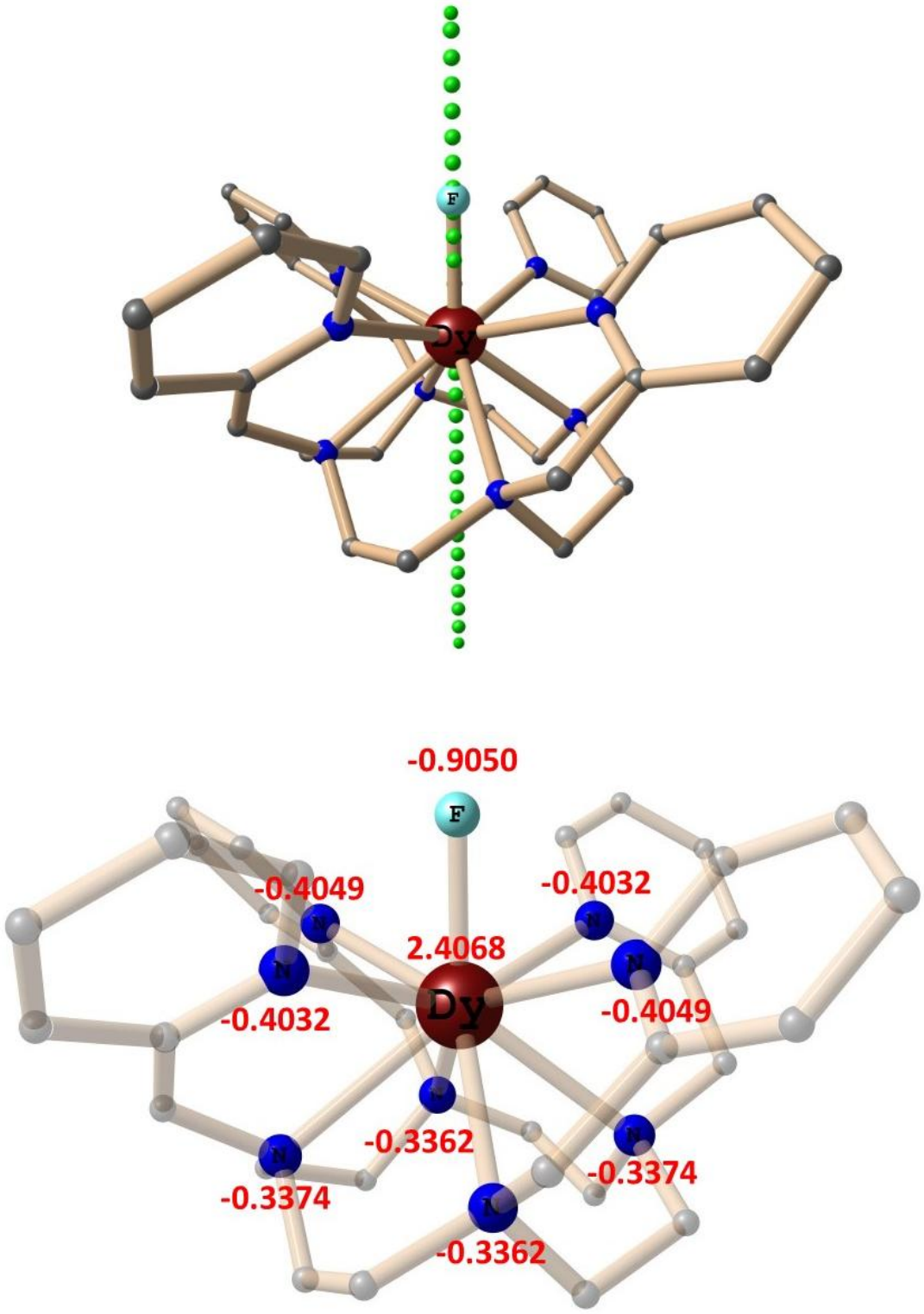

Fig. S28 (upper) *Ab initio* SINGLE_ANISO computed ground state KD orientation along with (lower) LoProp charges of the important atoms for complex **1**.

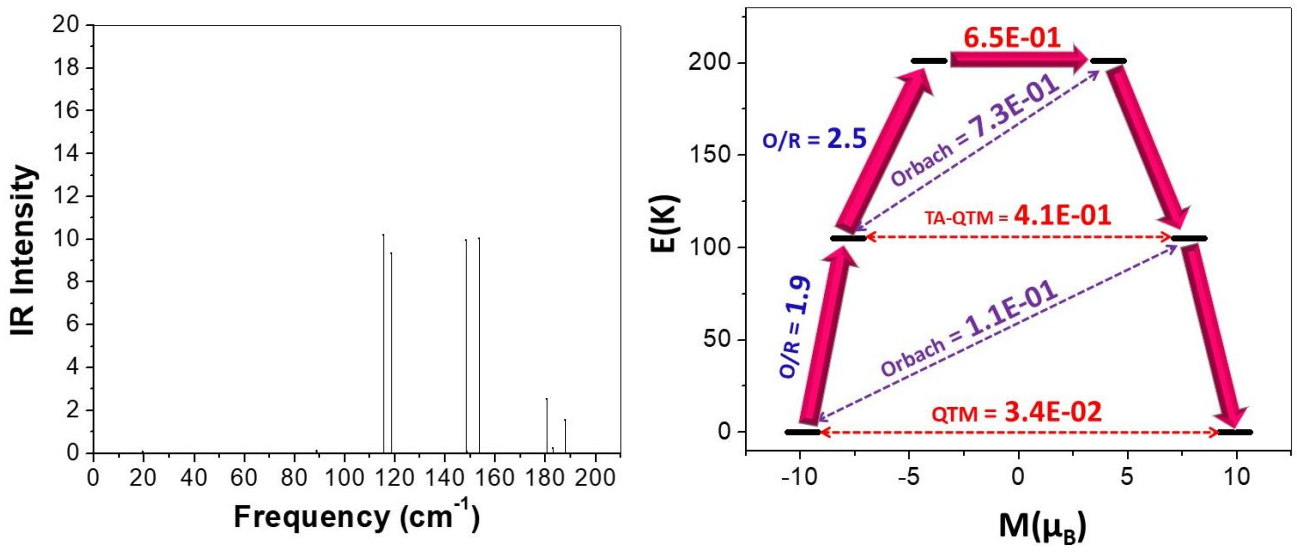

Fig. S29 (left) DFT calculated frequencies for complex **1**. The frequency at 115 cm^{-1} is the one through which one can expect relaxation. This frequency has Dy-F axial bond bending and very small stretching. We have performed magneto-structural studies on the models generated from this frequency. (right) Magnetic blockade diagram for model at a scale displacement of 1.5 Å, the U_{cal} value is reduced ≤203 K. It is important to note here that the change in Dy-F bond distance is very small at this scale displacement (~0.1 Å).

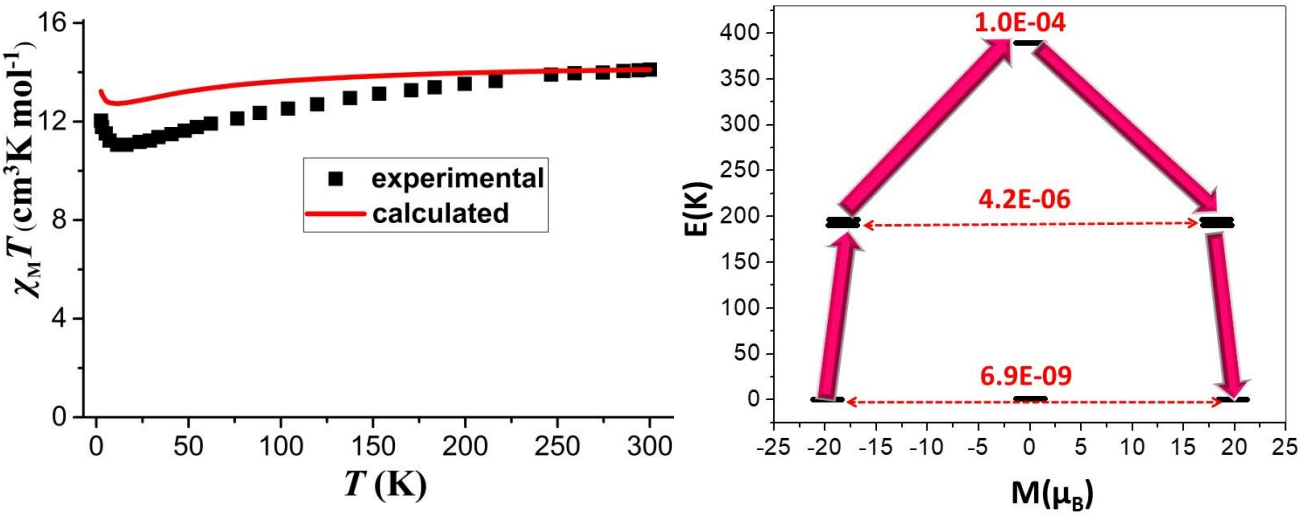

Fig. S30 (Left) *Ab initio* simulated (red line) and experimental (black squares) $\chi_M T$ vs. T plots for complex **1**. (Right) POLY_ANISO computed blockade diagram for complex **1**, when considering intermolecular exchange and dipolar exchange couplings (0.08 cm^{-1} and 0.02 cm^{-1}, respectively). The numbers given in the magnetic blockade diagram represent tunnel splittings for the non-Kramers *dimeric* Dy···Dy model system.

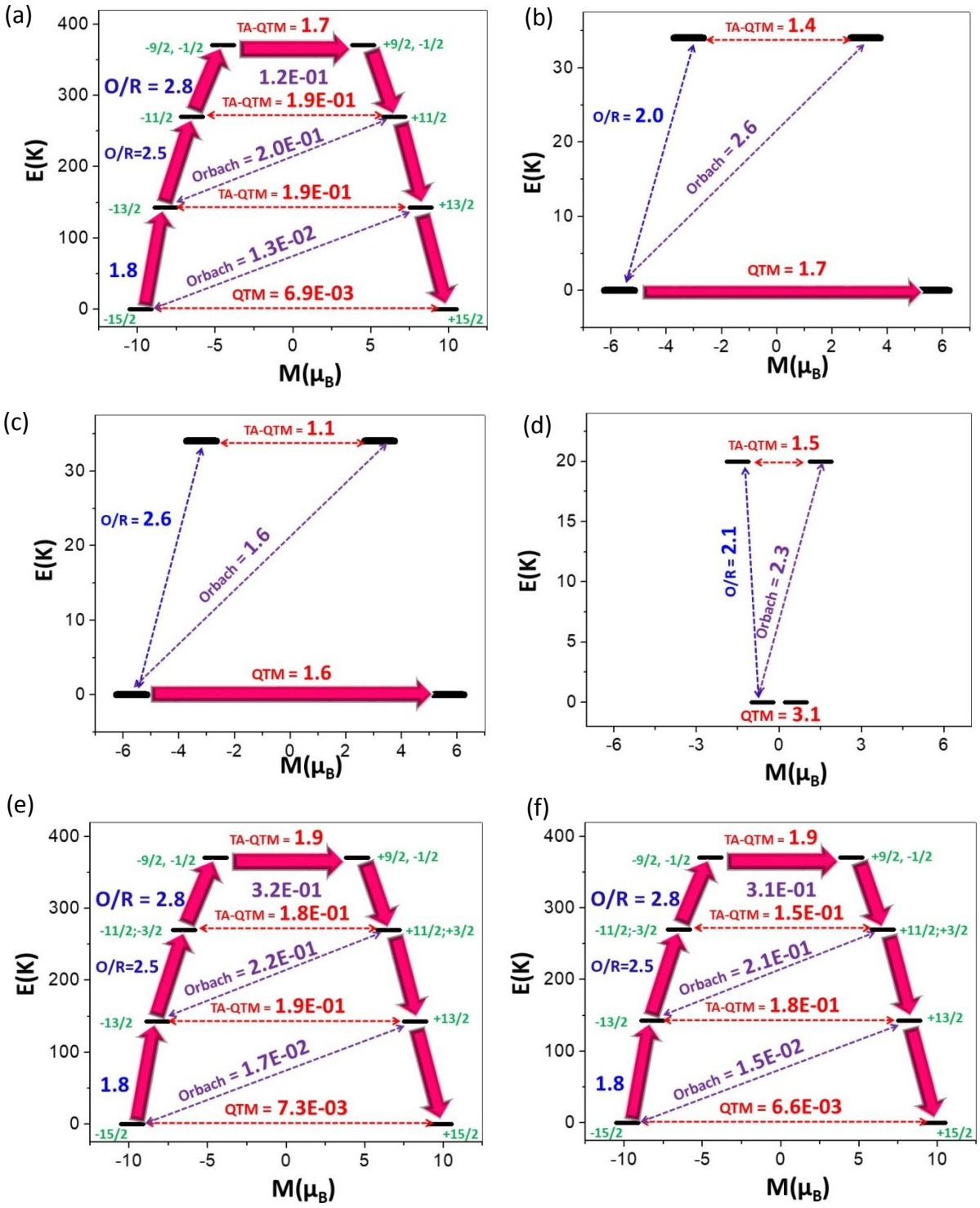
(a)
TA-QTM = 1.7
-9/2, -1/2
+9/2, -1/2
1.2E-01
O/R = 2.8
TA-QTM = 1.9E-01
-11/2
+11/2
O/R=2.5
Orbach = 2.0E-01
TA-QTM = 1.9E-01
-13/2
+13/2
1.8
Orbach = 1.3E-02
QTM = 6.9E-03
-15/2
+15/2
E(K)
M(μB)
(b)
TA-QTM = 1.4
O/R = 2.0
Orbach = 2.6
QTM = 1.7
E(K)
M(μB)
(c)
TA-QTM = 1.1
O/R = 2.6
Orbach = 1.6
QTM = 1.6
E(K)
M(μB)
(d)
TA-QTM = 1.5
O/R = 2.1
Orbach = 2.3
QTM = 3.1
E(K)
M(μB)
(e)
TA-QTM = 1.9
-9/2, -1/2
+9/2, -1/2
3.2E-01
O/R = 2.8
TA-QTM = 1.8E-01
-11/2;-3/2
+11/2;+3/2
O/R=2.5
Orbach = 2.2E-01
TA-QTM = 1.9E-01
-13/2
+13/2
1.8
Orbach = 1.7E-02
QTM = 7.3E-03
-15/2
+15/2
E(K)
M(μB)
(f)
TA-QTM = 1.9
-9/2, -1/2
+9/2, -1/2
3.1E-01
O/R = 2.8
TA-QTM = 1.5E-01
-11/2;-3/2
+11/2;+3/2
O/R=2.5
Orbach = 2.1E-01
TA-QTM = 1.8E-01
-13/2
+13/2
1.8
Orbach = 1.5E-02
QTM = 6.6E-03
-15/2
+15/2
E(K)
M(μB)

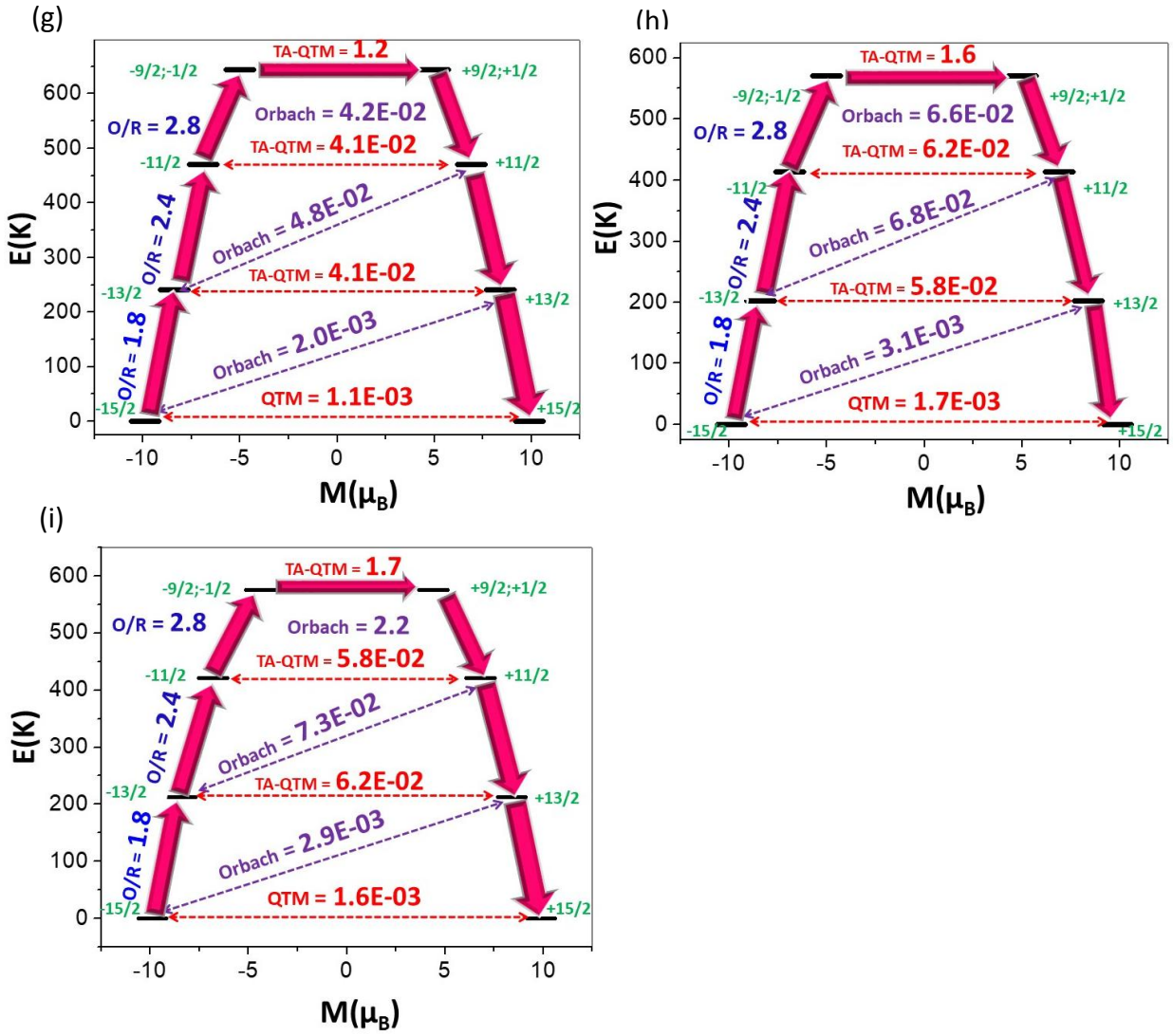

Fig. S31 *Ab initio* calculated relaxation dynamics for Models **1-9** (a-i, see Fig S32 and Table S8). The arrows show the connected energy states with the number representing the matrix element of the transverse moment (see text for details). Here, QTM = quantum tunnelling of the magnetisation, TA-QTM = thermally assisted QTM, O/R = Orbach/Raman process. The numbers above each arrow represent corresponding transverse matrix elements for the transition magnetic moments.

(a)

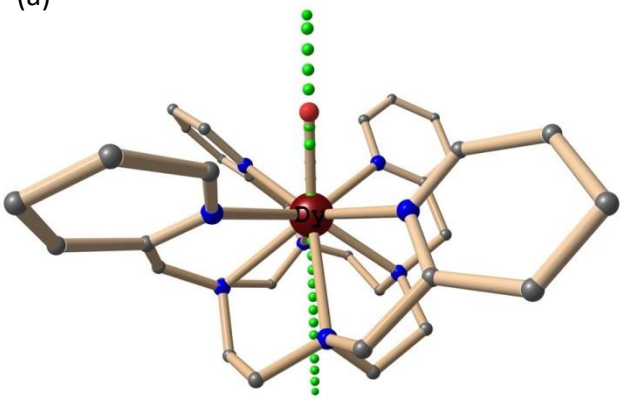

(b)

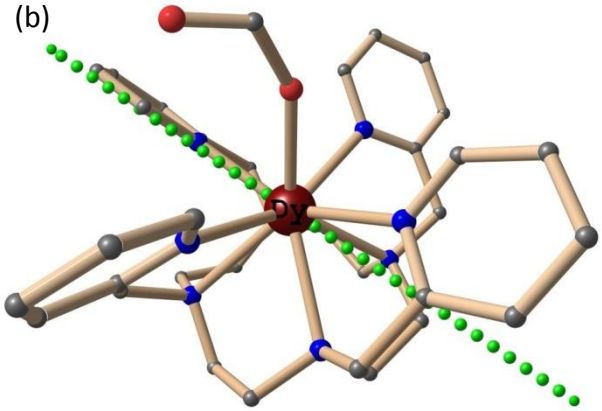

(c)

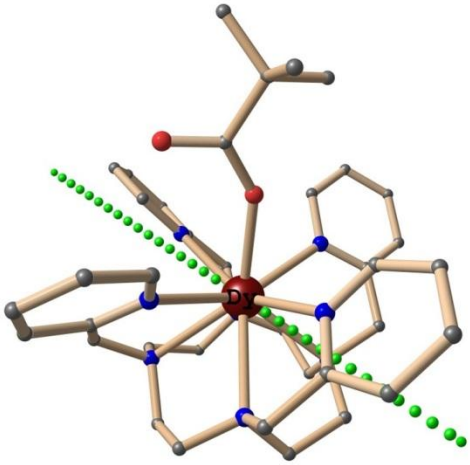

(d)

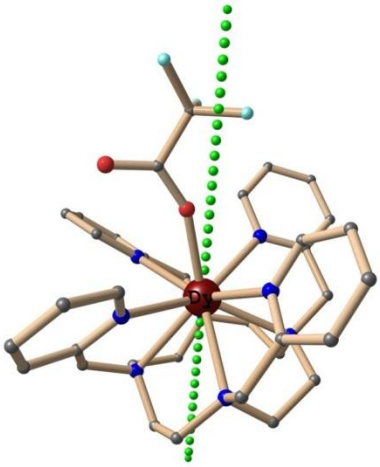

(e)

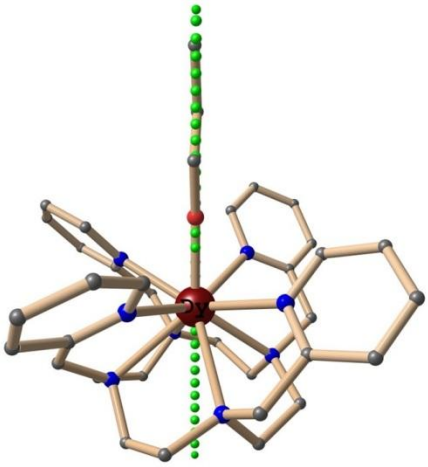

(f)

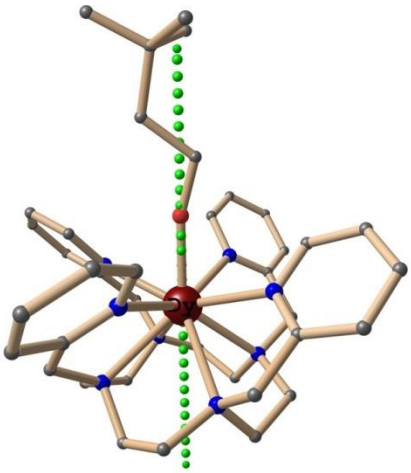

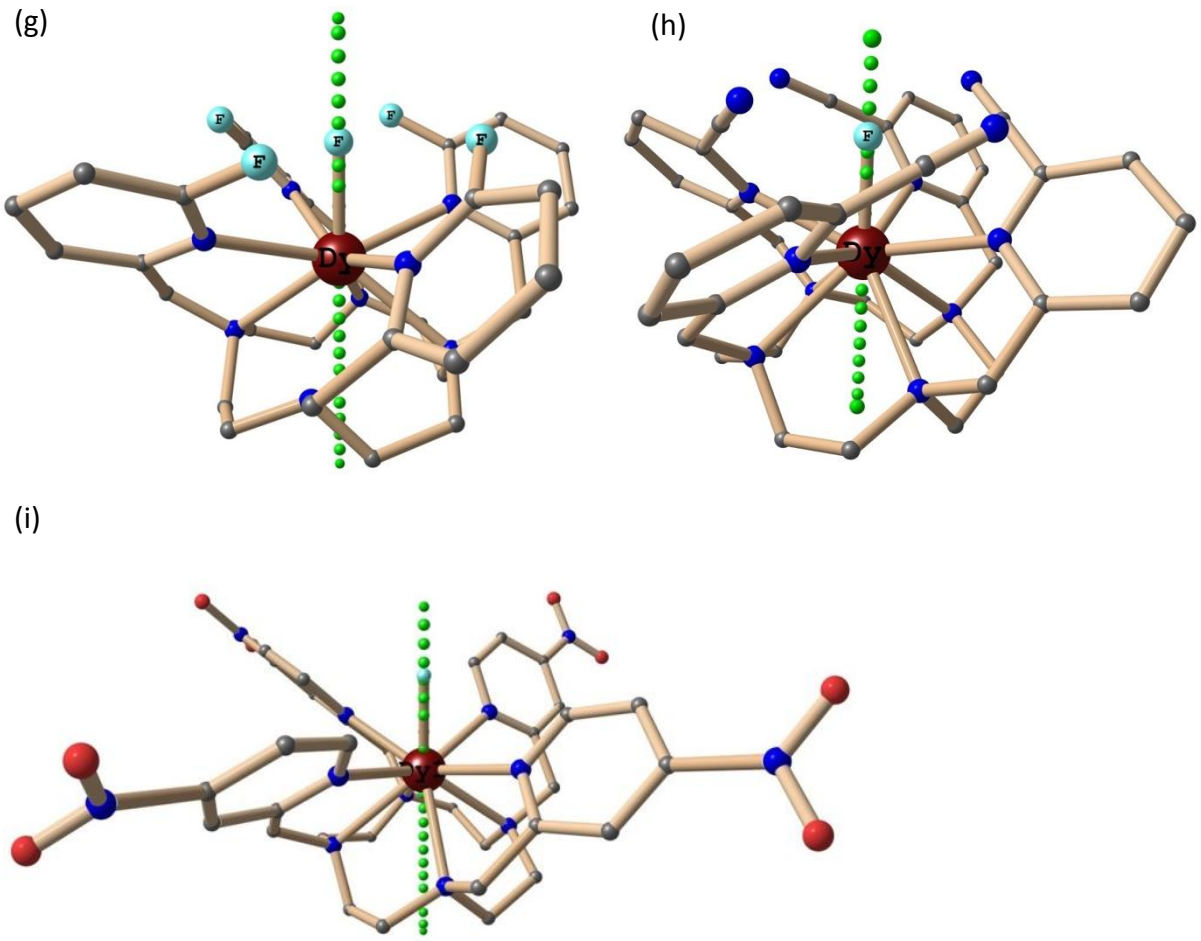

Fig. S32 *Ab initio* SINGLE_ANISO computed ground state KD orientation for Models **1**-**9**.

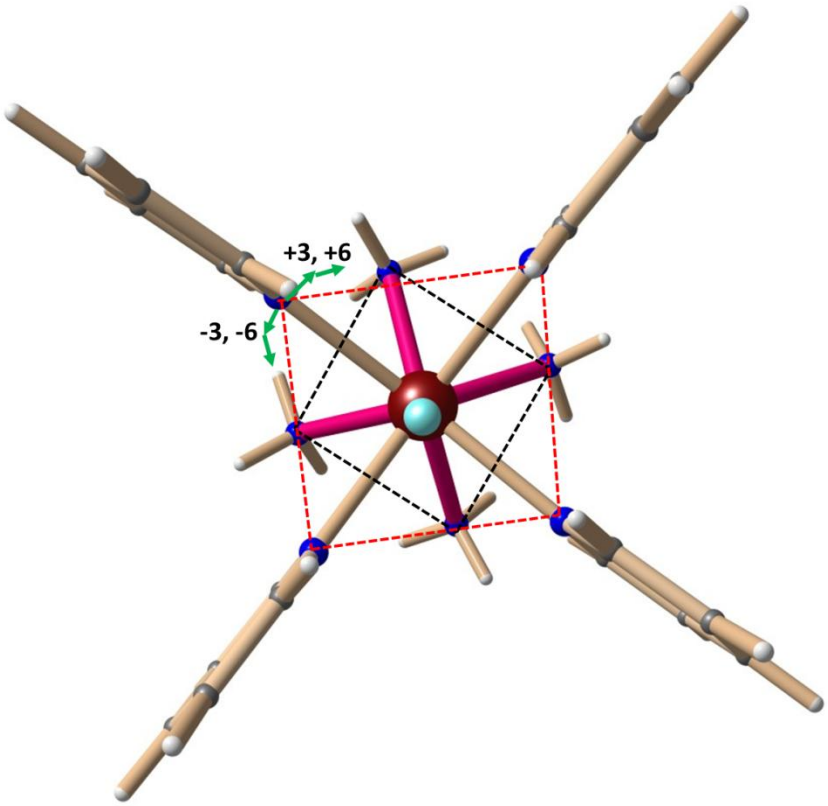

ModelA±X	U_{cal} (K)
ModelA	382
ModelA-3	384
ModelA-6	385
ModelA+3	380
ModelA+6	382

Fig. S33 ModelA (top) on which magneto-structural studies have been performed by rotating the -N_4 plane. *Ab initio* U_{cal} values are given in the Table. The changes in the U_{cal} values are very small suggesting the dominance of the strong axial ligand field over the transverse field, upon rotating the -N_4 plane.

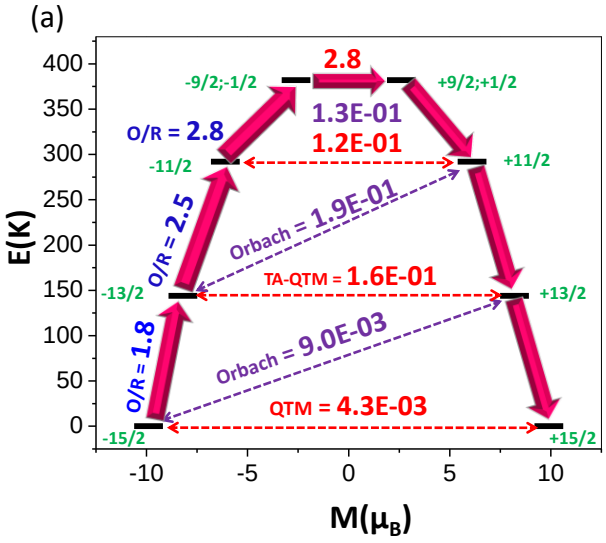
(a)
E(K)
M(μB)
-9/2;-1/2
+9/2;+1/2
-11/2
+11/2
-13/2
+13/2
-15/2
+15/2
2.8
1.3E-01
1.2E-01
O/R = 2.8
O/R = 2.5
O/R = 1.8
Orbach = 1.9E-01
TA-QTM = 1.6E-01
Orbach = 9.0E-03
QTM = 4.3E-03

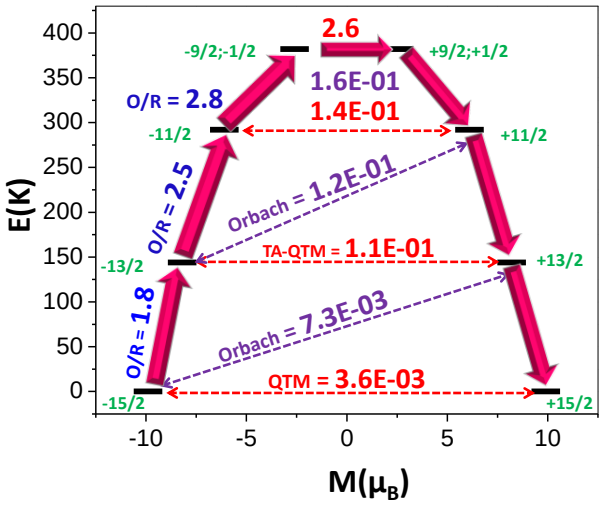
(b)
E(K)
M(μB)
-9/2;-1/2
+9/2;+1/2
-11/2
+11/2
-13/2
+13/2
-15/2
+15/2
2.6
1.6E-01
1.4E-01
O/R = 2.8
O/R = 2.5
O/R = 1.8
Orbach = 1.2E-01
TA-QTM = 1.1E-01
Orbach = 7.3E-03
QTM = 3.6E-03

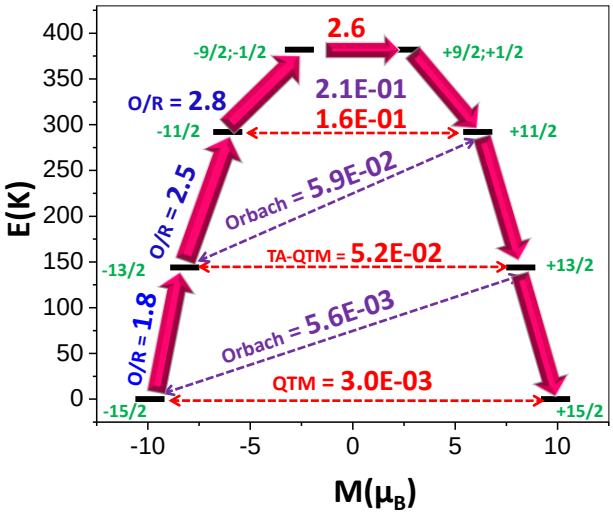
(c)
E(K)
M(μB)
-9/2;-1/2
+9/2;+1/2
-11/2
+11/2
-13/2
+13/2
-15/2
+15/2
2.6
2.1E-01
1.6E-01
O/R = 2.8
O/R = 2.5
O/R = 1.8
Orbach = 5.9E-02
TA-QTM = 5.2E-02
Orbach = 5.6E-03
QTM = 3.0E-03

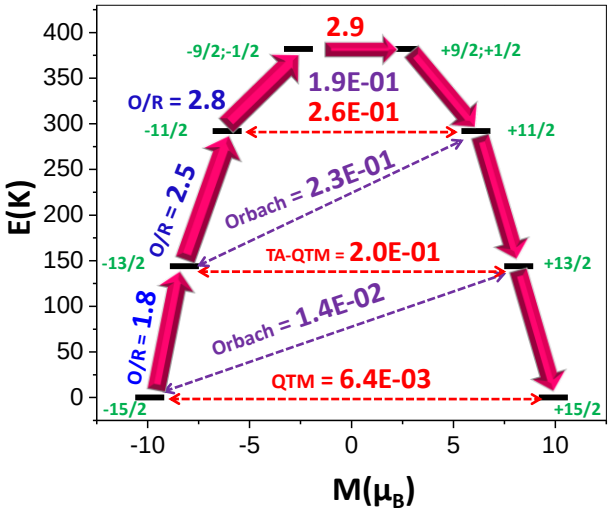
(d)
E(K)
M(μB)
-9/2;-1/2
+9/2;+1/2
-11/2
+11/2
-13/2
+13/2
-15/2
+15/2
2.9
1.9E-01
2.6E-01
O/R = 2.8
O/R = 2.5
O/R = 1.8
Orbach = 2.3E-01
TA-QTM = 2.0E-01
Orbach = 1.4E-02
QTM = 6.4E-03

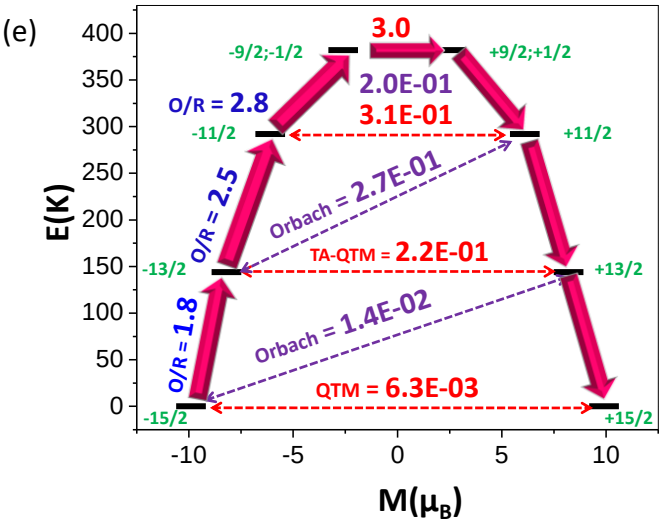
(e)
E(K)
M(μB)
-9/2;-1/2
+9/2;+1/2
-11/2
+11/2
-13/2
+13/2
-15/2
+15/2
3.0
2.0E-01
3.1E-01
O/R = 2.8
O/R = 2.5
O/R = 1.8
Orbach = 2.7E-01
TA-QTM = 2.2E-01
Orbach = 1.4E-02
QTM = 6.3E-03

Fig. S34 (a-e) Magnetic blockade diagram for ModelA, ModelA-3, ModelA-6, Model+A3 and Model+A6 respectively. Rotation of the -N4 plane does not change the U_{cal} as well as the QTM/TA-QTM values, suggesting the dominance of the strong axial Dy-F bond.

References

1. L. S. Natrajan, N. M. Khoabane, B. L. Dadds, C. A. Muryn, R. G. Pritchard, S. L. Heath, A. M. Kenwright, I. Kuprov and S. Faulkner, *Inorg. Chem.,* 2010, **49**, 7700.
2. W. Wernsdorfer, *Supercond. Sci. Technol.*, 2009, **22**, 064013; W. Wernsdorfer, N. E. Chakov, and G. Christou, *Phys. Rev. B.,* 2004, **70**, 132413; W. Wernsdorfer, *Adv. Chem. Phys*., 2001, **118**, 99.
3. S. P. Westrip, *J. Apply. Cryst.*, 2010, **43**, 920.
4. M. Llunell, D. Casanova, J. Cirera, P. Alemany and S. Alvarez, Shape Program, Version 2.0, 2010
5. L. Sun, S. Zhang, Z. Jiang, Q. Yang, S. Chen, Y. Zhang, W. Wang, Q. Weia and G. Xie, *Dalton Trans*., 2017, **46**, 11159.
6. P-H. Lin, I. Korobkov, T. J. Burchell and M. Murugesu*, Dalton Trans*., 2012, **41**, 13649.
7. Z.-X. Jiang, J.-L. Liu, Y.-C. Chen, J. Liu, J.-H. Jia and M.-L. Tong, *Chem. Commun*., 2016, **52**, 6261.
8. N. F. Chilton, S. K. Langley, B. Moubaraki, A. Soncini, S. R. Batten and K. S. Murray, *Chem. Sci.*, 2013, **4**, 1719.
9. E. L. Gavey, M. Al Hareri, J. Regier, L. D. Carlos, R. A. S. Ferreira, F. S. Razavi, J. M. Rawsond and M. Pilkington, *J. Mater. Chem*. *C*, 2015,**3**, 7738.
10. S. She, G. Su, B. Wang, Q. Lei, Y. Yang, L. Gong and B. Liu, *Eur. J. Inorg. Chem*., 2017, 2406.
11. S. Goswami, S. Biswas, K. Tomar and S. Konar, *Eur. J. Inorg. Chem*., 2016, 2774.
12. V. E. Campbell, H. ne Bolvin, E. Riviere, R. Guillot, W. Wernsdorfer and T. Mallah, *Inorg. Chem.* 2014, **53**, 2598.
13. P. Antal, B. Drahoš, R. Herchel and Z. Trávníček, *Dalton Trans*., 2016,**45**, 15114.
14. L.-F. Wang, J.-Z. Qiu, J.-L. Liu, Y.-C. Chen, J.-H. Jia, J. Jover, E. Ruiz and M.-L. Tong, *Chem. Commun*., 2015, **51**, 15358.
15. L. Sun, S. Zhang, C. Qiao, S. Chen, B. Yin, W. Wang, Q. Wei, G. Xie and S. Gao, *Inorg. Chem*., 2016, **55** 10587.
16. D. Hamada, T. Fujinami, S. Yamauchi, N. Matsumoto, N. Mochida, T. Ishida, Y. Sunatsuki, M. Tsuchimoto, C. Coletti, N. Re, *Polyhedron*, 2016, **109**, 120.

17. J. Jung, X. Yi, G. Huang, G. Calvez, C. Daiguebonne, O. Guillou, O. Cador, A. Caneschi, T. Roisnel, B. Le Guennic and K. Bernot, *Dalton Trans*., 2015, **44**, 18270.
18. G.-J. Chen, C.-Y. Gao, J.-L. Tian, J. Tang, W. Gu, X. Liu, S.-P. Yan, D.-Z. Liao and P. Cheng, *Dalton Trans*., 2011, **40**, 5579.
19. H. R. Wen, F.-Y. Liang, Z.-G. Zou, S.-J. Liu, J.-S. Liao, J.-L. Chen; *Inorg. Chem. Commun*., 2017, **79**, 41.
20. J. Ruiz, A. J. Mota, A. R.-Dieguez, S. Titos, J. M. Herrera, E. Ruiz, E. Cremades, J. P. Costes and E. Colacio, *Chem. Commun*., 2012, 48, 7916.
21. V. E. Campbell, R Guillot, E. Riviere, P.-T. Brun, W. Wernsdorfer and T. Mallah, *Inorg. Chem*., 2013, **52**, 5194.
22. F. Gao, F.-L. Yang, X. Feng, H. Xu, W. Sun, H. Liu and X.-L. Li, *Dalton Trans.*, 2017, **46**, 1317.
23. E. Lucaccini, M. Briganti, M. Perfetti, L. Vendier, J.-P. Costes, F. Totti, R. Sessoli and L. Sorace, *Chem. Eur. J.,* 2016, **22**, 5552.
24. J.-R. Jiménez, I. F. D.-Ortega, E. Ruiz, D. Aravena, S. J. A. Pope, E. Colacio and J. M. Herrera, *Chem.Eur.J.,* 2016, **22**, 14548.
25. G. Peng, Y. –Y. Zhang, Z. –Y. Li, *Inorg. Chem. Commun*., 2017, **77**, 40.
26. L. Norel, L. E. Darago, B. Le Guennic, K. Chakarawet, M. I. Gonzalez, J. H. Olshansky, S. Rigaut and J. R. Long, *Angew. Chem. Int. Ed*. 2018, **57**, 1.
27. M. U. Anwar, L. N. Dawe, S. S. Tandon, S. D. Bunge and L. K. Thompson, *Dalton Trans*., 2013, **42**, 7781.
28. L. J. Batchelor, Irene Cimatti, R. Guillot, F. Tuna, W. Wernsdorfer, L. Ungur, L. F. Chibotaru, V. E. Campbell and T. Mallah, *Dalton Trans.*, 2014, **43**, 12146.
29. M. Guo, Y. Wang, J. Wu, L. Zhao and J. Tang, *Dalton Trans.*, 2017, **46**, 564.
30. Y.-S. Ding, T. Han, Y.-Q. Hu, M. Xu, S. Yang and Y.-Z. Zheng, *Inorg. Chem. Front*., 2016, **3**, 798.
31. A. K. Mondal, S. Goswami and S. Konar, *Dalton Trans.,* 2015, **44**, 5086.
32. P. Chen, M. Zhang, W. Sun, H. Li, L. Zhao and P. Yan, *CrystEngComm*, 2015,**17**, 5066.
33. A. Upadhyay, C. Das, S. Vaidya, S. Kumar Singh, T. Gupta, R. Mondol, S. K. Langley, K. S. Murray, G. Rajaraman and M. Shanmugam, *Chem.Eur.J.* 2017, **23**, 4903.
34. D. Maniaki, I. M.-Margaritis, J. Mayans, A. Savvidou, C. P. Raptopoulou, V. Bekiari, V. Psycharis, A. Escuer and S. P. Perlepes, *Dalton Trans*., 2018, **47**, 11859.
35. K. R. Meihaus, S. G. Minasian, W. W. Lukens, S. A. Kozimor, D. K. Shuh, T. Tyliszczak and J. R. Long, *J. Am. Chem. Soc*., 2014, **136**, 6056; J. M., Zadrozny, Mihail Atanasov, Aimee M. Bryan, Chun-Yi Lin, Brian D. Rekken, Philip P. Power, Frank Neese and J. R. Long, *Chem. Sci*., 2013, **4**, 125.
36. D. Gatteschi, R. Sessoli and J. Villain, Molecular Nanomagnets, Oxford University Press, New York, 2006; E. Rousset, M. Piccardo, M,-E, Boulon, R.W. Gable, A. Soncini, L. Sorace and C. Boskovic, *Chem.Eur.J.* 2018, **24**, 14768; Y-S. Ding, K-X. Yu, D. Reta, F. Ortu, R. E.P. Winpenny, Y.-Z. Zheng and N. F. Chilton,

Nat. Commun., 2018, **9**, 3134; A. Abragam and B. Bleaney, *Electron Paramagnetic Resonance of Transition Ions*; Oxford University Press: Oxford, UK, 1970.

37. F. Aquilante, L. De Vico, N. Ferré, G. Ghigo, P.-å. Malmqvist, P. Neogrády, T. B. Pedersen, M. Pitoňák, M. Reiher, B. O. Roos, L. Serrano-Andrés, M. Urban, V. Veryazov and R. Lindh, *J. Comput. Chem.*, 2010, **31**, 224-247.

38. M. J. Frisch, G. W. Trucks, H. B. Schlegel, G. E. Scuseria, M. A. Robb, J. R. Cheeseman, G. Scalmani, V. Barone, B. Mennucci, G. A. Petersson, H. Nakatsuji, M. Caricato, X. Li, H. P. Hratchian, A. F. Izmaylov, J. Bloino, G. Zheng, J. L. Sonnenberg, M. Hada, M. Ehara, K. Toyota, R. Fukuda, J. Hasegawa, M. Ishida, T. Nakajima, Y. Honda, O. Kitao, H. Nakai, T. Vreven, J. A. Montgomery, J. E. Peralta, F. Ogliaro, M. Bearpark, J. J. Heyd, E. Brothers, K. N. Kudin, V. N. Staroverov, R. Kobayashi, J. Normand, K. Raghavachari, A. Rendell, J. C. Burant, S. S. Iyengar, J. Tomasi, M. Cossi, N. Rega, J. M. Millam, M. Klene, J. E. Knox, J. B. Cross, V. Bakken, C. Adamo, J. Jaramillo, R. Gomperts, R. E. Stratmann, O. Yazyev, A. Austin, J. R. Cammi, C. Pomelli, J. W. Ochterski, R. L. Martin, K. Morokuma, V. G. Zakrzewski, G. A. Voth, P. Salvador, J. J. Dannenberg, S. Dapprich, A. D. Daniels, Ö. Farkas, J. B. Foresman, J. V. Ortiz, J. Cioslowski and D. J. Fox, Gaussian 09, 2009.
39. C. Lee, W. Yang, R. G. Parr, *Phys. Rev. B: Condens. Matter* **1988,** *37*, 785; A. D. Becke, *J. Chem. Phys.* **1993,** *98*, 5648; A. D. Becke, *J. Chem. Phys.***1993,** *98*, 1372; P. J. Stephens, F. J. Devlin, F. C. Chabalowski, M. J. Frisch, *J. Phys. Chem.* **1994,** *98*, 11623.
40. M. Dolg, U. Wedig, H. Stoll and H. Preuss, *J. Chem. Phys*., **1987**, *86*, 866.
41. P. C. Hariharan and J. A. Pople, *Theor. chim. acta*, **1973**, *28*, 213.